Available online at www.sciencedirect.com
ScienceDirect
Geochimica et Cosmochimica Acta 70 (2006) 5013–5034
Geochimica
www.elsevier.com/locate/gca

# The chemical-temporal evolution of lithospheric mantle underlying the North China Craton

Fu-Yuan Wu [a,*], Richard J. Walker [b], Yue-Heng Yang [a], Hong-Lin Yuan [c], Jin-Hui Yang [a]

[a] State Key Laboratory of Lithospheric Evolution, Institute of Geology and Geophysics, Chinese Academy of Sciences, Qijiahuozi, 100029 Beijing, China
[b] Isotope Geochemistry Laboratory, Department of Geology, University of Maryland, College Park, Maryland 20742, USA
[c] State Key Laboratory of Continental Dynamics, Department of Geology, Northwest University, Xi'an 710069, China

Received 22 February 2006; accepted in revised form 17 July 2006

**Abstract**

Previous studies of samples of subcontinental lithospheric mantle (SCLM) that underlay the North China Craton (NCC) during the Paleozoic have documented the presence of thick Archean SCLM at this time. In contrast, samples of SCLM underlying the NCC during the Cenozoic are characterized by evidence for melt depletion during the Proterozoic, and relatively recent juvenile additions to the lithosphere. These observations, coupled with geophysical evidence for relatively thin lithosphere at present, have led to the conclusion that the SCLM underlying the NCC was thinned and modified subsequent to the late Paleozoic. In order to extend the view into both the Paleozoic and modern SCLM underlying the NCC, we examine mantle xenoliths and xenocrystic chromites extracted from three Paleozoic kimberlites (Tieling, Fuxian and Mengyin), and mantle xenoliths extracted from one Cenozoic basaltic center (Kuandian). Geochemical data suggest that most of the Kuandian xenoliths are residues of small degrees of partial melting from chemically primitive mantle. Sr–Nd–Hf isotopic analyses indicate that the samples were removed from long-term depleted SCLM that had later been variably enriched in incompatible elements. Osmium isotopic compositions of the two most refractory xenoliths are depleted relative to the modern convecting upper mantle and have model melt depletion ages that indicate melt depletion during Paleoproterozoic. Other relatively depleted xenoliths have Os isotopic compositions consistent with the modern convecting upper mantle. This observation is generally consistent with earlier data for xenoliths from other Cenozoic volcanic systems in the NCC and surrounding cratons. Thus, the present SCLM underlying the NCC has a complex age structure, but does not appear to retain materials with Archean melt depletion ages. Results for what are presumed to be early Paleozoic xenoliths from Teiling are generally highly depleted in melt components, e.g. have low $Al_2O_3$, but have also been metasomatically altered. Enrichment in light rare earth elements, low $\varepsilon_{Nd}$ values ($\sim -10$), and relatively high $^{87}Sr/^{86}Sr$ (0.707–0.710) are consistent with a past episode of metasomatism. Despite the metasomatic event, $^{187}Os/^{188}Os$ ratios are low and consistent with a late Archean melt depletion event. Thus, like results for xenoliths from other early Paleozoic volcanic centers within the NCC, these rocks sample dominantly Archean SCLM. The mechanism for lithospheric thinning is still uncertain. The complex age structure currently underlying the NCC requires either variable melt depletion over the entire history of this SCLM, or the present lithospheric material was partly or wholly extruded under the NCC from elsewhere by the plate collisions (collision with the Yangtze Craton and/or NNW subduction of the Pacific plate) that may have caused the thinning to take place.


## 1. Introduction

Studies of the eastern portion of the North China Craton (NCC) (Fig. 1a), have proposed that a significant part of the original underlying subcontinental lithospheric mantle (SCLM) was removed subsequent to the early Paleozoic (e.g. Menzies et al., 1993). This conclusion was based on the occurrence and characteristics of early Paleozoic diamondiferous kimberlites in Mengyin of the Shandong Province (central eastern China) and Fuxian of the Liaoning Province (northeastern China) (Fig. 1a). The presence of these diamond-bearing rocks implies the existence of thick (≈200 km) SCLM at the time of volcanism (Fan and Menzies, 1992; Menzies et al., 1993; Chi and Lu,

* Corresponding author. Fax: +86 10 62007932.
*E-mail addresses:* wufuyuan@mail.igcas.ac.cn (F.-Y. Wu), rjwalker@geol.umd.edu (R.J. Walker).

0016-7037/$ - see front matter © 2006 Elsevier Inc. All rights reserved.
doi:10.1016/j.gca.2006.07.014

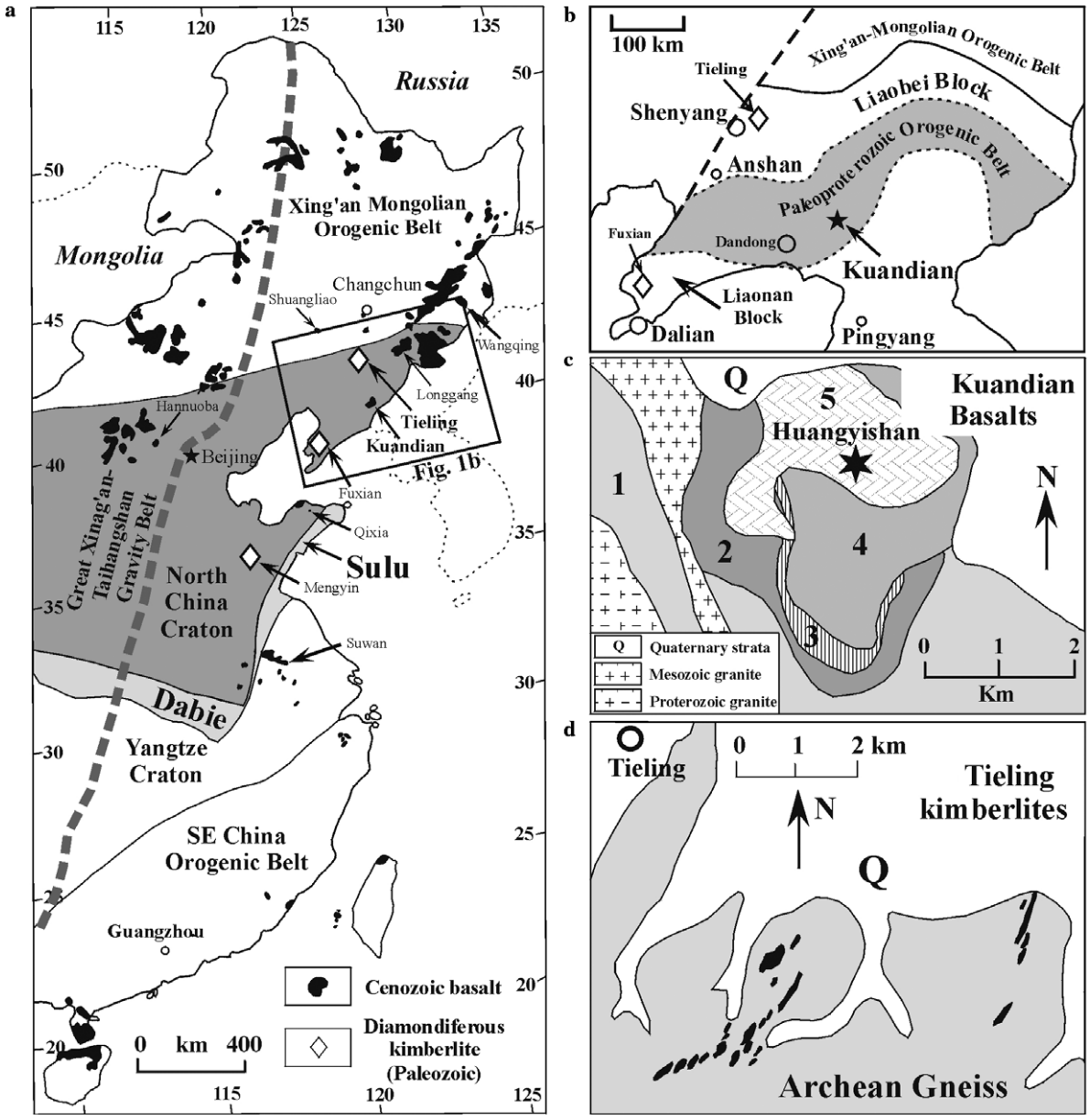


Fig. 1. Simplified distribution map of Cenozoic volcanic rocks in Eastern China (a). Paleozoic and Cenozoic volcanic rocks from the North China Craton (NCC) where mantle xenoliths were sampled by Gao et al. (2002a) (Fuxian, Hannuoba, and Qixia) and Wu et al. (2003) (Longgang, Wangqing, and Shuangliao) are also shown for comparison. Kuandian volcanoes and Tieling kimberlites are located in the Liaodong Peninsula (b). The Huangyishan volcano is composed of five stages of eruptions of basaltic magma (c), and the Tieling kimberlites are composed of 26 veins (d).

1996; Griffin et al., 1998; Wang et al., 1998). Furthermore, isotopic data for mantle xenoliths entrained in these kimberlites indicate that at least some portions of the SCLM at that time recorded Archean melt depletion ages (Gao et al., 2002a). In contrast, geophysical data, and isotopic studies of mantle xenoliths taken from Cenozoic basalts reveal that the present lithosphere is much thinner (60–120 km) and may also be younger (Menzies et al., 1993; Griffin et al., 1998; Menzies and Xu, 1998).

Lithospheric thinning of the NCC has been attributed by some studies to result from thermal-mechanical erosion of the SCLM (Menzies et al., 1993; Xu, 2001; Xu et al., 2004). If so, this could result in present SCLM that is a mixture of juvenile and ancient materials. In contrast, other studies that have focused on compositions of the Mesozoic high-Mg lavas, mineral compositions and Sr–Nd isotopic compositions of mantle xenoliths from this region, have concluded that a significant portion of the SCLM was delaminated (Deng et al., 1994; Wu and Sun, 1999; Wu et al., 2000; Gao et al., 2004). This would require that the present SCLM was partly or entirely added from the ambient convecting upper mantle subsequent to thinning. In this case, the SCLM may be dominated by mantle similar to the depleted source of mid-ocean ridge basalts (DMM).

The age structure of the SCLM underlying the NCC, however, remains unclear due in part to scarce age data from a limited number of locations. For example, Os isoto-

pic data for only three mantle xenoliths from two Paleozoic kimberlites have been reported (Gao et al., 2002a), so it remains unclear whether Archean SCLM was prevalent under the NCC during the Paleozoic. Furthermore, the significance of Proterozoic model ages from some mantle xenoliths transported to the surface by Cenozoic volcanism remains poorly understood (Wu et al., 2003). Does the presence of this material require a Proterozic replacement of Archean SCLM that has survived until the present? Was this material added to the SCLM as part of the natural growth process for lithospheric mantle? Or was Proterozoic lithospheric mantle that formed elsewhere somehow added after the Paleozoic?

The objectives of this study are to expand the geographical sampling of SCLM xenoliths in the NCC and to further examine the age/composition structure of the SCLM underlying that region. Towards that end, we have examined mantle xenoliths from the Cenozoic Kuandian basalts, located in the Liaoning Province of the northeastern portion of the NCC (Fig. 1a–b). This location is about 300 km to the north of the Paleozoic Fuxian kimberlite. In addition, peridotites from Tieling, in the same province, approximately 200 km to the north of Kuandian, were examined (Fig. 1d). These xenoliths are of great interest because they are present in kimberlites that are very similar to the Paleozoic kimberlites at Fuxian and Mengyin. Although the age of these kimberlites is not well constrained at present, the presence of diamonds in some require that they formed pre-lithospheric thinning. In addition, some chromite megacrysts from Fuxian, Mengyin and Tieling kimberlites, presumably mechanically separated from mantle xenoliths being transported by the kimberlites, are also analyzed in order to further constrain the nature of the SCLM prior to lithospheric thinning.

## 2. Geological background

Eastern China is composed of the Xing'an-Mongolian orogenic belt and the NCC in the north, the Dabie-Sulu ultrahigh-pressure collisional belt in the central region, and the Yangtze Craton and Southeastern China Orogenic Belt in the south (Fig. 1a). The NCC is the oldest tectonic unit in China, containing crust as old as 3800 Ma (Liu DY et al., 1992). Neodymium $T_{DM}$ model ages of felsic rocks are generally Archean and range mainly between 2.5 and 2.9 Ga, but with two age peaks at 2.6–2.8 Ga and 3.2–3.6 Ga (Wu et al., 2005a). The Liaodong Peninsula is located in the eastern segment of the NCC (Fig. 1a) and can be subdivided into three tectonic units: the Archean Liaonan (southern Liaoning) block in the south, the Archean Liaobei (northern Liaoning) block in the north and the Paleoproterozoic (Liaoji) orogenic belt between them (Faure et al., 2004; Luo et al., 2004; Fig. 1b). The Liaonan and Liaobei blocks are composed of a series of late Archean diorite–tonalite–granodiorite suites that are extensively deformed and contain minor supracrustal rocks. Neodymium isotopic model ages for these rocks are mainly between 2800 and 2500 Ma, although 3800 Ma crust has been found near Anshan (Liu DY et al., 1992). Between the two blocks, the Paleoproterozoic strata were deposited and then metamorphosed during a 1.85 Ga orogenic event (Lu et al., 2006), considered to be the time of cratonization of the NCC (Zhao et al., 2005). Subsequently, the Liaodong Peninsula was covered by thick sequences of Meso- to Neoproterozoic and Paleozoic sediments. A sedimentary gap developed during the early- to middle-Paleozoic ($O_1$–$C_2$). The Fuxian, Mengyin and presumably Tieling kimberlites were formed during this period with the former having a phlogopite Rb–Sr isochron age of ~460 Ma (Dobbs et al., 1994).

Since the late Mesozoic, eastern China has become an important part of the circum–Pacific tectonic–magmatic zone. During this time, intensive deformation, mineralization, and igneous activity occurred, including extensive eruption of intermediate-acid volcanic rocks and widespread emplacement of granites (Wu et al., 2005b,c).

During the Cenozoic, the NCC has been characterized by extensive intraplate basaltic volcanism. Some of these basalts contain ultramafic xenoliths that have been the focus of numerous studies (e.g E and Zhao, 1987; Chi, 1988; Zhou et al., 1988; Fan and Hooper, 1989; Liu CQ et al., 1992; Tatsumoto et al., 1992; Fan et al., 2000). Ultramafic xenoliths are mostly found in Neogene and Quaternary alkaline basalts, and are generally not found in tholeiitic flows, or in late Cretaceous–Paleogene basalts (Fan and Hooper, 1989).

## 3. Sample descriptions

The Kuandian volcanic field contains more than 20 Quaternary volcanoes with eruption ages of less than 0.6 Ma (Fig. 1c; LBGMR, 1989; Xie et al., 1992). Samples were collected from the Huangyishan volcano. According to published data, the basaltic rocks of this volcanic field are alkaline and are enriched in light and depleted in heavy rare earth elements (REE), interpreted as indicating derivation from relatively deep mantle with garnet in the residue (Liu CQ et al., 1992). Mantle xenoliths of peridotites and pyroxenites, and megacrysts of garnet and clinopyroxene are widely distributed, with diameters ranging mostly between 30 and 80 cm in the 1st, 2nd and 4th lava flows, and associated pyroclastic deposits (Fig. 1c; Lu et al., 1983; LBGMR, 1989; Tatsumoto et al., 1992). Spinel lherzolite is the dominant rock type in the Huangyishan xenolith suite with minor harzburgite, typical of other basaltic localities in eastern China and world-wide (Fan and Hooper, 1989; Pearson et al., 2003). The xenoliths are mostly coarse-grained and equigranular, with occasional porphyroblastic textures, but no strongly foliated types. The rocks are generally fresh and do not contain secondary alteration minerals. Primary minerals are clinopyroxene (16–3%), orthopyroxene (31–23%), olivine (75–52%) and spinel (3–1%). Sample HY2-06 contains approximately 2% amphibole, indicating modification via aqueous-rich fluid and/

or melt metasomatism (Ionov et al., 1997; Downes, 2001; Pearson et al., 2003).

The Tieling kimberlites were intruded into Archean gneiss in the Liaobei Block (Fig. 1a and d). According to the regional geological survey of Yu (1987), 26 kimberlitic pipes have been identified. Although diamond is sparingly present, no major occurrences for any pipe have been reported. The eruption age of the kimberlites is presently unknown. Griffin et al. (1998) proposed that these kimberlites could be of Cretaceous–Tertiary age. Because the Tieling kimberlites have the same petrological and geochemical characteristics as those in Mengyin and Fuxian (Chi and Lu, 1996), we speculate that their eruption ages may have been coeval (at 460 Ma), consistent with the conclusions of Lu et al. (1995). Consequently, because of the similarities with the known Paleozoic kimberlites, we will hereafter assume eruption occurred at approximately the same time (460 Ma) as for Mengyin and Fuxian. A well constrained age of formation is not necessary for the purposes here, although may ultimately be critical for containing the timing of the lithospheric thinning. The identification of occasional diamond in the kimberlites indicates that the lithosphere was thick when the kimberlites erupted (≈150 km or greater, Chi and Lu, 1996), so as with the Mengyin xenoliths, there is little doubt that the kimberlites, and the included xenoliths sample the SCLM that existed prior to thinning. The Tieling xenoliths present in some of the Tieling kimberlites have diameters ranging mostly from about 10 to 30 cm and were intensively serpentinized and carbonatized, similar to those at Mengyin and Fuxian. Only relict chromites are identified.

As a means of building a larger database for the SCLM of the NCC, we also analyzed chromite megacrysts from the previously studied Paleozoic kimberlites, Fuxian and Mengyin, and also analyzed a chromite megacryst from Tieling. The assumption is that the chromite megacrysts were mechanically separated from the very rare peridotitic xenoliths present in these volcanic systems. Chromite was targeted for study here because it is normally characterized by high Os concentrations and very low Re/Os (e.g. Walker et al., 2002). These characteristics would make it an ideal phase with which to place high confidence constraints on Os model melt depletion ages of the mantle beneath these volcanic sites.

## 4. Analytical techniques

### 4.1. Elemental analyses

The xenolith samples studied here were first crushed using a corundum jaw crusher, then small chips without surface alteration were selected to make powders, using an agate mortar. Elemental analyses were conducted at the Department of Geology, Northwest University in Xi'an, China. Major element analyses of whole-rock powders were determined using a RIGAKU 2100 X-ray fluorescence (XRF) instrument. Thirty-eight standards, ranging from ultramafic to felsic rocks and sediments, were used to construct calibration curves. During the digestion of the standards and samples, 0.5 g of powder were mixed with 3.6 g of $Li_2B_4O_7$, 0.4 g of LiF, 0.3 g of $NH_4NO_3$ and a small quantity (<20 mg) of LiBr. A glass bead was formed via fusion. The current and voltage during analyses were 50 mA and 50 kV, respectively. According to the measured values of standards (GSR-1 and GSR-3), the uncertainties are ~±1% for elements with concentrations >1.0 wt%, and about ±10% for the elements with concentrations <1.0 wt%.

Trace element concentrations, including the REE, were determined using a PE Elan 6000 inductively-coupled plasma mass spectrometer (ICP-MS). About 50 mg of crushed whole-rock powder was dissolved using $HF/HNO_3$ (2:1) mixtures in a Teflon bomb, which was heated on a hot plate at ~140 °C. This was followed by evaporation to dryness, refluxing with 1.5 mL HF and 1.5 mL $HNO_3$ before sealing and placing in a steel jacket, and heating in an oven at 190 °C for 48 h. The third step was evaporating the solution to dryness, dissolving it with 3 mL $HNO_3$, and drying it again. Then, 3 mL $HNO_3$ was added before it was again sealed and heated at 140 °C for 12 h. Finally, the solution was extracted after cooling, and diluted to 80 g. External standards BHVO-1, AGV-1 and G-2 were used to monitor drift in mass response during mass spectrometric measurement.

### 4.2. Mineral compositional analyses

Mineral major element compositions were obtained using a *JEOL-JAX8100* microprobe with 15 kV accelerating potential and 12 nA beam current at the Department of Geology, Peking University. Counting times were 20 s. Total iron is expressed as FeO.

Mineral trace element compositions (including REE) were made via laser ablation inductively-coupled plasma mass spectrometry (LA-ICP-MS) at the Northwest University, China. Detailed analytical procedures are provided in Gao et al. (2002b). The ICP-MS used was an *Elan 6100* from *Perkin-Elmer/SCIEX*. The instrument offered a sensitivity of ca. 90 million counts per second (cps) for 1 μg/mL of In (indium) when used in the standard solution nebulization mode (Meinhard concentric nebulizer and cyclonic spray chamber). Background intensities were usually a few cps for elements above $m/z = 85$ (Rb), except for Sn and Pb, which may reach 100–200 cps due to memory effects.

A *GeoLas 200 M* laser-ablation system was used for the laser ablation measurements. The system is equipped with a 193 nm ArF-excimer laser and a homogenizing, imaging optical system. The set-up delivers a flat top beam onto the sample surface and the laser wavelength and energy density (40 J/cm$^2$) allows controlled ablation of highly transparent samples. A 30 μm spot size was used for this study. Helium was used as the carrier gas to enhance transport efficiency of ablated material. The

helium carrier gas inside the ablation cell is mixed with argon as a makeup gas before entering the ICP to maintain stable and optimum excitation conditions. The measurements were carried out using time resolved analysis operating in a fast, peak hopping sequence in dual detector mode. Each spot analysis consisted of approximately 30 s background acquisition (gas blank) followed by 60 s data acquisition from the sample. Calibration was performed using NIST SRM 610 as an external calibration sample in conjunction with internal standardization using Ca.

### 4.3. Sr–Nd–Hf isotopic analyses

Strontium, Nd and Hf isotopic analyses of clinopyroxenes from Kuandian and whole-rock xenoliths from Tieling were conducted at the MC-ICPMS Laboratory, Chinese Academy of Sciences, Beijing, using a Thermo-Electron Neptune multi-collector-ICPMS. For Sr and Nd isotopes, ~150 mg of sample were dissolved in sealed Savillex™ beakers for more than 2 weeks. Separation of Sm and Nd was done using a routine two-column ion exchange technique which includes: (1) a group separation of light REE through a cation exchange column ($1 \times 8$ cm, packed with Bio-Rad AG50X8, 200–400 mesh resin), and (2) a purification of Sm and Nd through a second exchange column ($0.6 \times 7$ cm) packed with Kel-F teflon powder with an exchange medium of HDEHP. For Hf isotopes, 200 mg of sample powder was used to make a similar glassy bead as described previously for XRF analyses. The glassy bead was digested in 3 N HCl, and then Hf was separated using Ln resin.

$^{87}Sr/^{86}Sr$, $^{143}Nd/^{144}Nd$ and $^{176}Hf/^{177}Hf$ ratios were normalized to $^{86}Sr/^{88}Sr = 0.1194$, $^{146}Nd/^{144}Nd = 0.7219$ and $^{179}Hf/^{177}Hf = 0.7325$. In the course of this study, two analyses of the NBS-987 Sr standard yielded $^{87}Sr/^{86}Sr = 0.710264 \pm 12$ and $0.710262 \pm 13$. Two analyses of the Lo Jolla Nd standard yielded $^{143}Nd/^{144}Nd = 0.511845 \pm 12$ and $0.511850 \pm 14$. One analysis of the JMC 475 Hf standard gave value of $^{176}Hf/^{177}Hf = 0.282159 \pm 7$. During the period of data acquisition, BCR-1 was also processed for Sr–Nd–Hf isotopes, and gave ratios of $0.705128 \pm 11$ for $^{87}Sr/^{86}Sr$, $0.512619 \pm 8$ for $^{143}Nd/^{144}Nd$ and $0.282861 \pm 3$ for $^{176}Hf/^{177}Hf$, all agreeing well with the recommended values.

### 4.4. Re–Os isotopic analyses

The chemical-separation techniques used in this study for Re–Os analysis are those of Shirey and Walker (1995). About 2 g of whole rock powder, a spike of mixed $^{185}Re$ and $^{190}Os$, and approximately 9 g of *aqua regia* were sealed inside Carius tubes, and heated at 280 °C for two days to obtain sample-spike equilibration. Osmium was purified using a carbon tetrachloride ($CCl_4$) solvent extraction technique (Cohen and Waters, 1996) followed by microdistillation purification. The Os total processing blank was $3 \pm 2$ pg and was inconsequential for all measurements. Rhenium was separated and purified from the matrix by using two successive anion exchange columns (200–400 mesh) with resin volumes of 0.8 and 0.1 mL, respectively. The samples were loaded and eluted on columns using 0.1 N $HNO_3$, Re was then collected using 6 M $HNO_3$, and then dried under a heat lamp (<80 °C). The Re blank for this procedure was $8 \pm 2$ pg.

Purified Os was then loaded using $Ba(OH)_2$ as an emission enhancer on platinum filaments and analyzed by negative thermal ionization mass spectrometry at the University of Maryland, College Park. Mass spectrometric procedures have been discussed in Walker et al. (1994, 2002). Most of the analyses in this paper were conducted in a static mode using six Faraday cups on a *VG Sector 54* thermal ionization mass spectrometer. For these levels of Os (2–5 ng), external reproducibility in the $^{187}Os/^{188}Os$ ratio was about ±0.1% (2$\sigma$), based on repeated analyses of comparable quantities of a standard. Rhenium analyses were determined using a *Nu Plasma* multi-collector-ICP-MS at the University of Maryland. In-run precisions were typically ±0.1 to 0.3% (2$\sigma$). Repeated measurements of an internal Re standard give an external precision of approximately ±0.3% (2$\sigma$). Blank corrections limit absolute uncertainties for most samples with low Re abundances (<100 pg/g) to approximately ±20–30%.

## 5. Results

### 5.1. Whole-rock geochemistry

Kuandian peridotites range from refractory harzburgite to relatively fertile lherzolite. Ten fresh samples were analyzed for bulk composition (Electronic Annex EA-1). The gain of mass on ignition was ~0.5%, consistent with the oxidation of FeO to $Fe_2O_3$ being more significant than the loss of volatiles. This, in turn, indicates generally low degrees of alteration in the xenoliths. Whole-rock $SiO_2$ concentrations range from 43.2% to 45.4%, and MgO concentrations range from 38.3% to 45.8%, indicating that these xenoliths were plucked from generally fertile mantle (Palme and O'Neill, 2003). Eight of the ten peridotites examined have $Al_2O_3$ concentrations >2 wt%. Most lie along the oceanic trend of Boyd (1989). The two harzburgites plot in the depleted portion of the field (Fig. 2a).

Three distinct types of whole-rock REE patterns are present in this suite (Fig. 3a–c): (1) the two refractory harzburgites (HY1-01, HY2-05) and two clinopyroxe-poor lherzolites (HY2-01, HY2-06) are LREE-enriched, although with chondrite-normalized values for all REE less than 4. The amphibole-bearing rock HY2-06 has the highest abundances of the LREE (Fig. 3a); (2) the moderately fertile lherzolites (HY2-02, HY2-07, and HY2-14) are characterized by relatively flat chondrite normalized patterns with normalized values for all REE of ~1–2 (Fig. 3b); (3) the most fertile lherzolites (HY2-03, HY2-04, and HY2-29) are LREE-depleted (Fig. 3c). Trace element distribu-

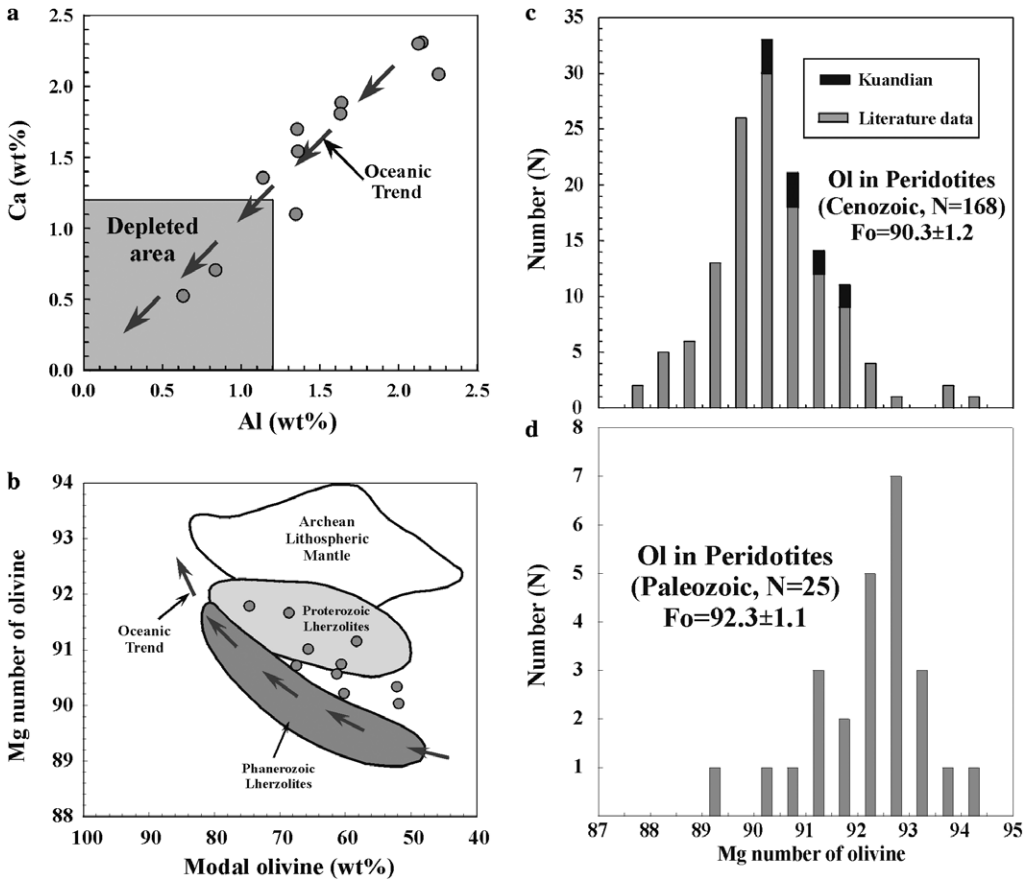


Fig. 2. (a) Plots of Ca (wt%) against Al (wt%) for the Kuandian peridotites. The oceanic trend and depleted area are from Boyd (1989) and are shown for comparison. (b) Modal olivine versus forsterite content in olivine in peridotites. Compiled fields for xenoliths found in Archean, Proterozoic and Phanerozoic terranes are from Boyd et al. (1997) and Griffin et al. (1999a). (c) Fo numbers of olivines in peridotite xenoliths found in Cenozoic basalts and (d) Fo numbers of olivines in peridotite xenoliths and diamonds found in Paleozoic kimberlites of Mengyin and Fuxian (modified after Wu et al., 2000).

tions for whole-rock samples normalized to primitive mantle are highly irregular (Fig. 3d–f). The LREE-enriched harzburgites have complex patterns, and contain generally higher concentrations of incompatible elements, with pronounced enrichments of La, Ce, Sr, Nd, and for some samples, Sm and Eu, compared to the other rocks from this suite (Fig. 3d). The moderately fertile lherzolites with relatively flat REE patterns are also characterized by similar primitive-mantle normalized values for other trace elements (Fig. 3e). In contrast, the most fertile, LREE-depleted lherzolites contain much lower abundances of most other incompatible elements, although here too, HY2-04 is anomalous with relative enrichments of Th, Nb along with La and Ce (Fig. 3f). As with peridotites worldwide (Pearson et al., 2003), the enrichments of incompatible elements are more pronounced in samples with relatively low heavy-REE (HREE) contents, and are coupled with the depletion of high field strength elements (HFSE) Zr, Hf, and Ti.

Among the seven Tieling xenoliths analyzed (Electronic Annex EA-2), loss of mass on ignition ranged from 15.5% to 26.1%, consistent with intensive alteration and addition of volatiles. If whole-rock compositions are recalculated excluding the ignition loss, $SiO_2$ concentrations range from 46.4% (FW04-351) to 31.8% (FW04-355), and MgO concentrations range from 40.3% (FW04-350) to 28.4% (FW04-354). The $Al_2O_3$ concentrations range from 0.87% (FW04-351) to 2.21% (FW04-355). In addition, sample FW04-354 has a much higher CaO content of 22.3% than other samples, indicating that this sample may have originally been an olivine–pyroxenite. Whole-rock REE patterns are similar for all samples, with major enrichment of LREE (Fig. 4a). Other trace element abundances within the Tieling suite are generally similar within suite. The Tieling peridotites contain higher concentrations of incompatible elements, with pronounced depletions of Nb, Zr, Hf, and Ti (Fig. 4b), so it is likely that the Tieling peridotites came from a melt-depleted, but subsequently metasomatically enriched mantle source.

### 5.2. Mineral chemistry and equilibration temperatures

The major element compositions of minerals from the Kuandian and spinels from the Tieling xenoliths are provided in Electronic Annex EA-3, and the trace element concentrations of clinopyroxene and amphibole are provided in Electronic Annex EA-4. The olivines have Fo numbers ranging from 90.2 to 91.7, and plot in the field of Protero-

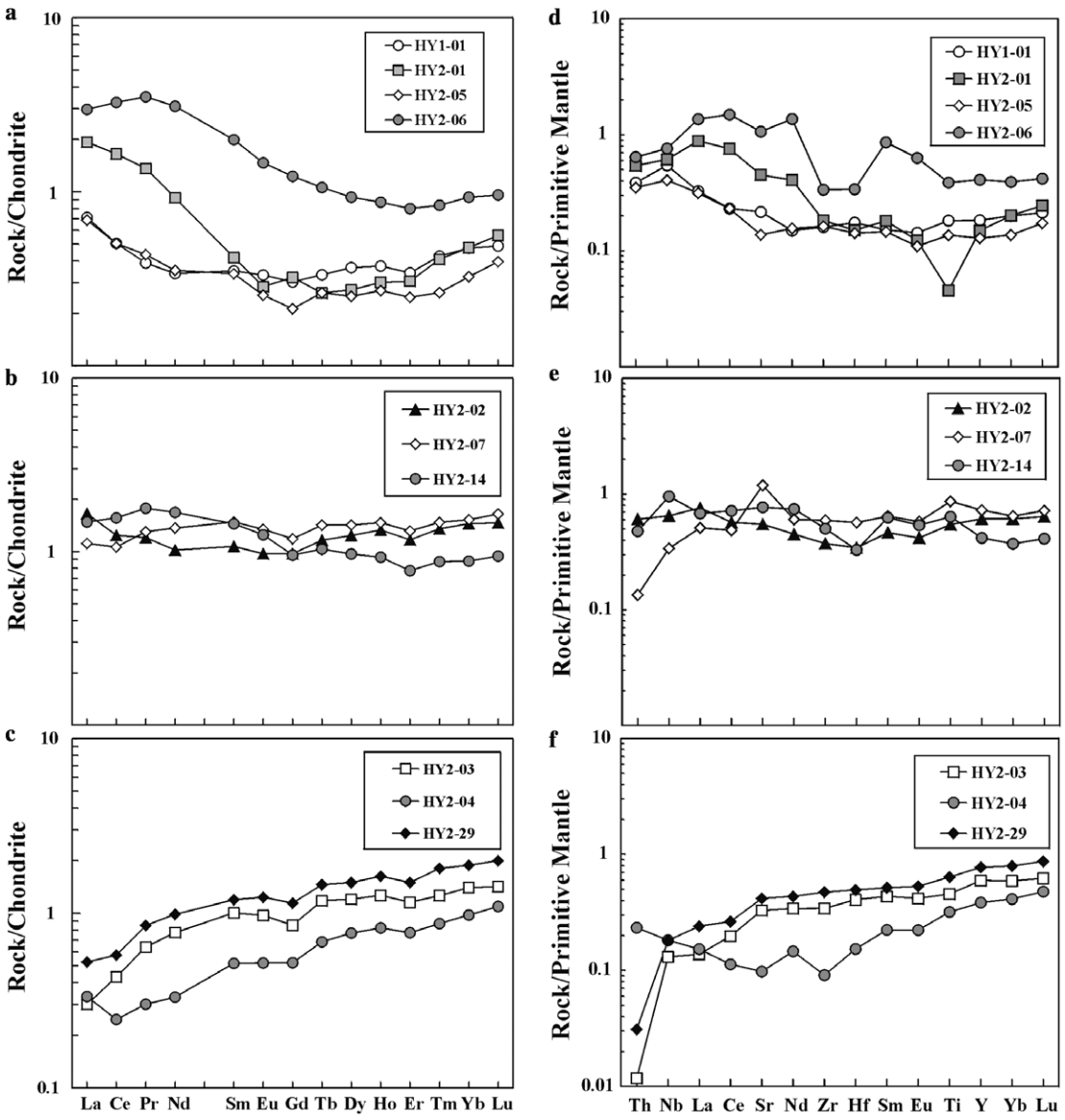


Fig. 3. Chondrite normalized rare earth element patterns (a–c) and primitive mantle normalized element patterns (d–f) for Kuandian peridotites. The trace elements are arranged in the order of decreasing incompatibility from left to right. The data were normalized to the values of Sun and McDonough (1989). The peridotites are divided into three groups based on REE pattern type.

zoic–Phanerozoic lithospheric mantle of Boyd (1989) and Griffin et al. (1999a) (Fig. 2b). The Fo compositions are also comparable with olivines from other Cenozoic locales in eastern China (Fig. 2c), but are significantly lower than those obtained from xenoliths transported by the Paleozoic kimberlites (Zheng, 1999) (Fig. 2d). The spinels from the Tieling xenoliths show much higher Cr/(Cr + Al) ratios of 41–91 than those from the Kuandian peridotites (9.0–28.5).

Rare earth and other trace element patterns for Kuandian clinopyroxenes are similar to the associated whole-rocks (Fig. 5a–f), indicating that clinopyroxene is the main host of most of the trace elements. There is some discrepancy, however, between whole-rock and clinopyroxe enrichments/depletions for Nb and Ti. For example, analyses of clinopyroxene in most samples show negative Nb and Ti anomalies, which are not observed in the bulk rocks. This may be related to the compensation effects of orthopyroxene, which can generate a positive Ti anomaly (Rampone et al., 1991; McDonough et al., 1992).

No compositional zoning has been detected in any of the clinopyroxene grains analyzed. It is noted that the clinopyroxenes from the depleted samples show significant depletions in Nb, Zr, Hf, and Ti in most cases. The amphibole from sample HY2-06 has the highest concentrations of most trace elements analyzed, but with relative depletions of Zr and Hf (Fig. 5a).

Using various geothermometers (Wood and Banno, 1973; Nehru and Wyllie, 1974; Lindsley and Dixon, 1975; Wells, 1977; Sachtleben and Seck, 1981; Bertrand and Mercier, 1985; Brey and Kohler, 1990), data for the 10 samples from Kuandian volcanoes indicate a large range of equili-

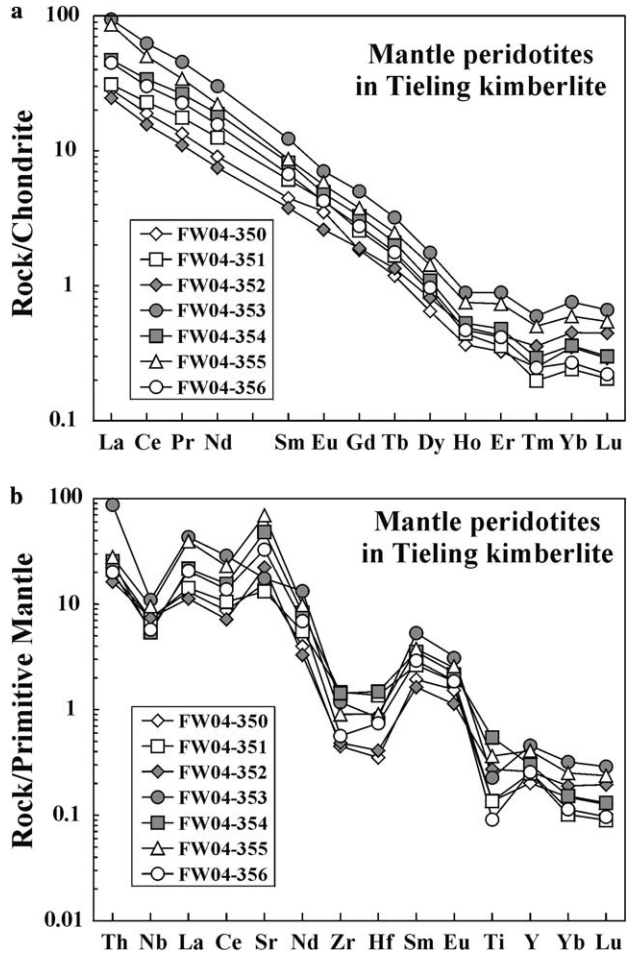


Fig. 4. Chondrite normalized rare earth element patterns (a) and primitive mantle normalized element patterns (b) for Tieling peridotites. The trace elements are arranged in the order of decreasing incompatibility from left to right. The normalized values are from Sun and McDonough (1989).

bration temperatures from 528 to 1236 °C (Electronic Annex EA-5). The temperature results obtained from the Wood and Banno (1973) and Bertrand and Mercier (1985) thermometers are systematically higher (from 954 to 1167 °C obtained from Wood and Banno (1973) and 873–1236 °C from Bertrand and Mercier (1985)), compared with 836–1096 °C obtained from the Wells (1977), and 807–1150 °C from Brey and Kohler (1990) thermometers. If the thermometer of Brey and Kohler (1990) is applied, the equilibrium temperature from these samples range from 807 °C to 1150 °C with most samples at 925–1150 °C. The amphibole-bearing sample of HY2-06 has the lowest equilibrium temperature of 807 °C.

The nearly complete replacement/recrystallization of primary minerals in the Tieling suite precludes the acquisition of usable primary mineral composition data for these rocks.

### 5.3. Sr–Nd–Hf isotopes

Previously published data for the Sr–Nd isotopic compositions of xenoliths from Kuandian have included analyses of peridotite, pyroxenite, megacryst (garnet, clinopyroxene, and amphibole) and host basalt (Liu CQ et al., 1992; Tatsumoto et al., 1992; Xu et al., 1998). The data for peridotites from this area, however, are limited, and it is not clear whether the analyses reported for megacrysts are from peridotite or pyroxenite. According to a survey (Fang and Ma, 1999), garnet only occurs in pyroxenite, but clinopyroxene and amphibole occur in both the peridotite and pyroxenite.

Our new Sr–Nd isotopic compositions of clinopyroxenes from Kuandian peridotites and whole-rocks from the Tieling peridotites are provided in Table 1. The clinopyroxenes from the Kuandian peridotites are characterized by generally low $^{87}Sr/^{86}Sr$ ratios of 0.7023–0.7045 and highly variable $\varepsilon_{Nd}$ with present day $\varepsilon_{Nd}$ values ranging from −3.4 to +26.2 (Fig. 6a). It is noted that the hornblende-bearing sample HY2-06 has the highest $^{87}Sr/^{86}Sr$ ratio of 0.7045 and negative $\varepsilon_{Nd}$ values of −3.4 among these peridotites. There is a crude negative correlation between $^{87}Sr/^{86}Sr$ and $\varepsilon_{Nd}$. It is clear that the Sr–Nd isotopic data of clinopyroxenes from the Kuandian peridotites are very different from Paleozoic and Mesozoic mafic rocks of the NCC, all of which are characterized by Sr–Nd systematics that are common to enriched mantle (Fig. 6a).

With the exception of sample of HY2-06, all Kuandian clinopyroxene data plot along a linear trend on a $^{143}Nd/^{144}Nd$ versus $^{147}Sm/^{144}Nd$ diagram (Fig. 6b). The meaning of this correlation is not clear, given that there is no reason to believe the samples are genetically related. If the data are regressed, an errorchron age of 358 ± 56 Ma is obtained (using ISOPLOT). The linearity may also result from mixing between two isotopically disparate components. Sample HY2-04, which is the most depleted in incompatible elements (Fig. 5f) and has the highest $^{147}Sm/^{144}Nd$ ratio of 0.601, gives a Nd $T_{DM}$ age of 320 Ma, similar to the regression age of the other samples. The other samples do not provide meaningful Nd model ages because they have $^{147}Sm/^{144}Nd$ ratios that are very similar to that of the depleted mantle.

The clinopyroxenes from the Kuandian xenoliths have $\varepsilon_{Hf}$ values that range from +15.2 to +88.6 (Fig. 6c), indicating derivation from long-term depleted mantle. In contrast to the Sm–Nd system, there is no correlation between $^{176}Lu/^{177}Hf$ and $^{176}Hf/^{177}Hf$ ratios (Fig. 6d). All Kuandian samples have $\varepsilon_{Nd}$–$\varepsilon_{Hf}$ values similar to or higher than the depleted mantle source of MORB except for amphibole-bearing HY2-06 (Fig. 6c). Most samples have meaningless $T_{DM}$ (Hf) ages because they have very similar $^{176}Lu/^{177}Hf$ ratios to the depleted mantle. However, sample HY2-04, which has the highest $^{176}Lu/^{177}Hf$ of 0.104, gives a Hf $T_{DM}$ age of 725 Ma, considerably older than its corresponding Nd model age. Variation plots of Sr–Nd–Hf isotopic composition versus indices of rock fertility (e.g. MgO concentrations of whole-rocks) (Fig. 7), reveal no correlation between $\varepsilon_{Nd}$ or $\varepsilon_{Hf}$ and MgO for the Kuandian peridotites. Samples with MgO of approximately 43 wt% have the highest $^{87}Sr/^{86}Sr$.

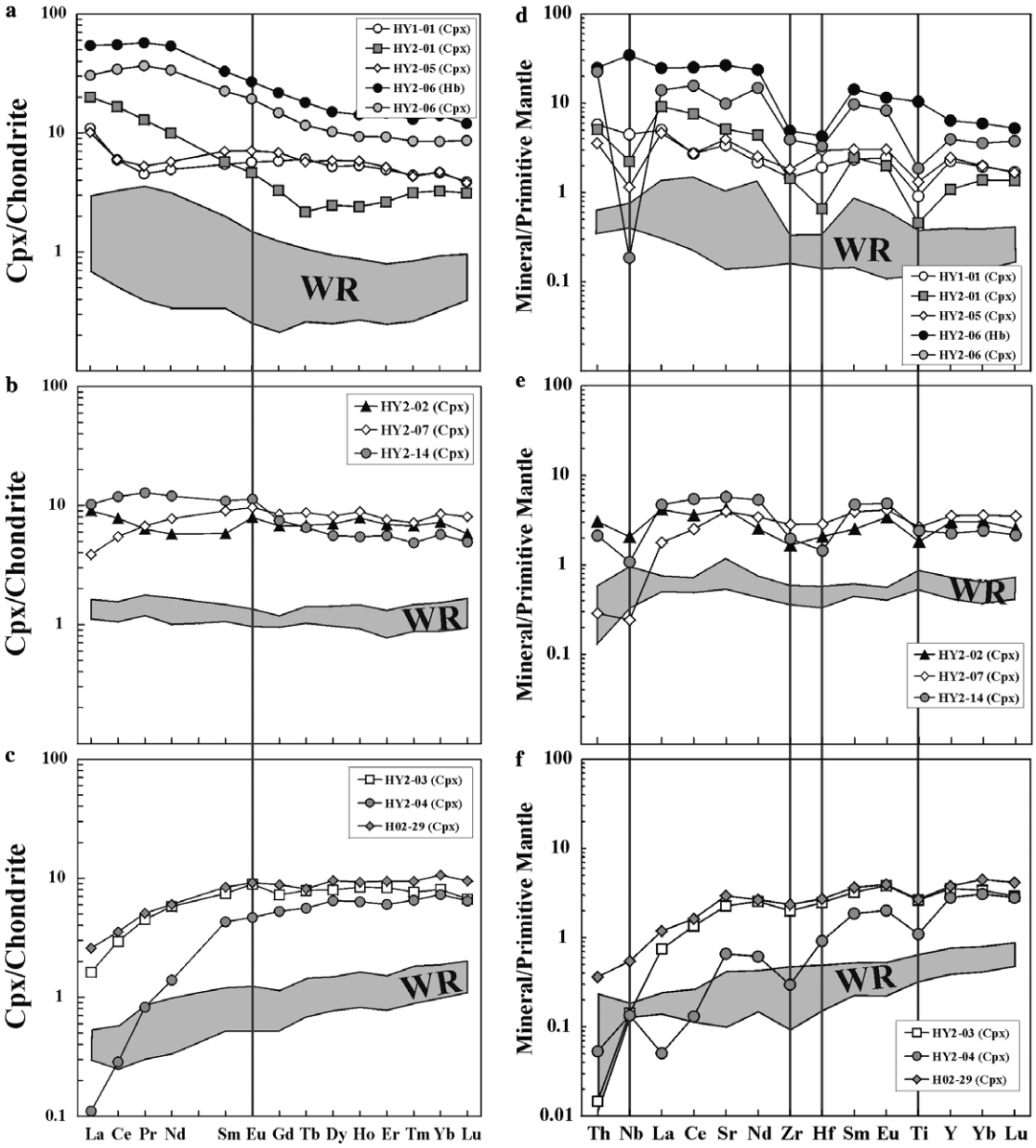


Fig. 5. Chondrite normalized rare earth element patterns (a–c) and primitive mantle normalized element patterns (d–f) for the clinopyroxenes and amphibole of Kuandian peridotites. The normalized values are from Sun and McDonough (1989).

Seven Tieling peridotites are characterized by high $^{87}Sr/^{86}Sr$ ratios of 0.7074–0.7101 and low $^{143}Nd/^{144}Nd$ ratios of 0.512094–0.512215 with $\varepsilon_{Nd}$ values ranging from −8.2 to −10.6 (Fig. 6a), comparable to the peridotites from Fuxian and Mengyin kimberlites (Chi and Lu, 1996; Zheng, 1999). Because of low Hf concentrations, Hf isotopic compositions were not determined for Tieling peridotites.

### 5.4. Re–Os isotopic systematics

Osmium and Re concentrations in the Kuandian peridotites range from 0.69 to 2.78 ppb, and from 0.01 to 0.21 ppb, respectively (Table 2). Samples HY2-02 and HY2-04 have Os concentrations of <1.0 ppb. Such low concentrations in peridotites are rare (e.g. Meisel et al., 2001), and have usually been attributed to melt percolation of S-undersaturated melts that remove Os-bearing sulfides (e.g. Reisberg et al., 2005). Low Os concentrations are often accompanied by more radiogenic Os isotopic compositions, suggestive of possible fluxing and Os exchange with oxidized melts or fluids (e.g. Brandon et al., 1996, 1999). The Os and Re concentrations for most of the Kuandian peridotites, however, are typical of worldwide occurrences of mantle peridotites. Kuandian samples have $^{187}Re/^{188}Os$ ratios ranging from 0.04 to 0.51, but nine of 10 samples have ratios less than the chondritic ratio of ~0.4. Six of the samples have very low ratios <0.1. Consequently, all

Table 1
Sr-Nd-Hf isotopic compositions of clinopyroxene separates of Kuandian peridotites and bulk samples of Tieling peridotites

| Sample | Location | t (Ma) | $^{87}Rb/^{86}Sr$ | $^{87}Sr/^{86}Sr$ | $2\sigma$ | $^{147}Sm/^{144}Nd$ | $^{143}Nd/^{144}Nd$ | $2\sigma$ | $^{176}Lu/^{177}Hf$ | $^{176}Hf/^{177}Hf$ | $2\sigma$ | $\varepsilon_{Nd(0)}$ | $\varepsilon_{Nd(t)}$ | $\varepsilon_{Hf(0)}$ | $T_{DM}$(Nd) (Ma) | $T_{DM}$(Hf) (Ma) |
|---|---|---|---|---|---|---|---|---|---|---|---|---|---|---|---|---|
| HY1-01 | Kuangdian | 0 | 0.0052 | 0.704030 | 12 | 0.2145 | 0.513248 | 16 | 0.0303 | 0.283500 | 18 | 11.9 | | 25.7 | 17554 | −1672 |
| HY2-01 | Kuangdian | 0 | 0.0029 | 0.703390 | 13 | 0.1112 | 0.512763 | 14 | 0.0705 | 0.285267 | 17 | 2.4 | | 88.2 | 576 | 3264 |
| Duplicate | | 0 | | 0.703343 | 25 | | 0.512761 | 10 | | 0.285278 | 40 | 2.4 | | 88.6 | 579 | 3281 |
| HY2-02 | Kuangdian | 0 | 0.0030 | 0.703031 | 15 | 0.1963 | 0.513101 | 8 | 0.0413 | 0.283365 | 9 | 9.0 | | 21.0 | 430 | 2081 |
| HY2-03 | Kuangdian | 0 | 0.0058 | 0.702941 | 13 | 0.2498 | 0.513199 | 9 | 0.0401 | 0.283347 | 8 | 10.9 | | 20.3 | 207 | 2948 |
| HY2-04 | Kuangdian | 0 | 0.0199 | 0.702680 | 40 | 0.6011 | 0.513948 | 10 | 0.1043 | 0.284148 | 41 | 25.6 | | 48.7 | 315 | 725 |
| Duplicate | | 0 | | 0.702813 | 19 | | 0.513983 | 13 | | | | 26.2 | | | 328 | |
| HY2-05 | Kuangdian | 0 | 0.0030 | 0.702900 | 15 | 0.2384 | 0.513123 | 12 | 0.0193 | 0.283587 | 21 | 9.5 | | 28.8 | −167 | −954 |
| HY2-06 | Kuangdian | 0 | 0.0009 | 0.704534 | 12 | 0.1295 | 0.512470 | 9 | 0.0389 | 0.283330 | 26 | −3.3 | | 19.7 | 1229 | 8649 |
| Duplicate | | 0 | | | | | 0.512464 | 11 | | 0.283296 | 8 | −3.4 | | 18.5 | 1240 | 5139 |
| HY2-07 | Kuangdian | 0 | 0.0026 | 0.702922 | 11 | 0.2262 | 0.513036 | 11 | 0.0418 | 0.283201 | 9 | 7.8 | | 15.2 | −1402 | −777 |
| HY2-14 | Kuangdian | 0 | 0.0017 | 0.704094 | 12 | 0.1766 | 0.512975 | 13 | 0.0507 | 0.283894 | 34 | 6.6 | | 39.7 | 720 | 2747 |
| HY2-29 | Kuangdian | 0 | 0.0036 | 0.702321 | 10 | 0.2724 | 0.513345 | 11 | 0.0519 | 0.283466 | 10 | 13.8 | | 24.5 | 507 | 852 |
| FW04-350 | Tieling | 460 | 0.0032 | 0.709055 | 18 | 0.0958 | 0.512107 | 11 | | | | −10.4 | −4.44 | | 1347 | |
| FW04-351 | Tieling | 460 | 0.0036 | 0.708684 | 15 | 0.0948 | 0.512118 | 11 | | | | −10.2 | −4.17 | | 1322 | |
| FW04-352 | Tieling | 460 | 0.0043 | 0.709427 | 14 | 0.0981 | 0.512183 | 16 | | | | −8.9 | −3.09 | | 1274 | |
| FW04-353 | Tieling | 460 | 0.0074 | 0.709077 | 16 | 0.0794 | 0.512094 | 8 | | | | −10.6 | −3.72 | | 1198 | |
| FW04-354 | Tieling | 460 | 0.0003 | 0.710099 | 9 | 0.0844 | 0.512146 | 30 | | | | −9.6 | −3.01 | | 1183 | |
| FW04-355 | Tieling | 460 | 0.0020 | 0.707439 | 6 | 0.0764 | 0.512104 | 9 | | | | −10.4 | −3.35 | | 1161 | |
| FW04-356 | Tieling | 460 | 0.0022 | 0.708172 | 12 | 0.0837 | 0.512215 | 70 | | | | −8.2 | −1.61 | | 1095 | |

t: eruption age of basalts/ kimberlites. $\varepsilon_{Hf} = ((^{176}Hf/^{177}Hf)_S/(^{176}Hf/^{177}Hf)_{CHUR} - 1) \times 10000$, where $(^{176}Lu/^{177}Hf)_S$ and $(^{176}Hf/^{177}Hf)_S$ are the measured values, $(^{176}Hf/^{177}Hf)_{CHUR} = 0.282772$ (Blichert-Toft and Albarede, 1997).

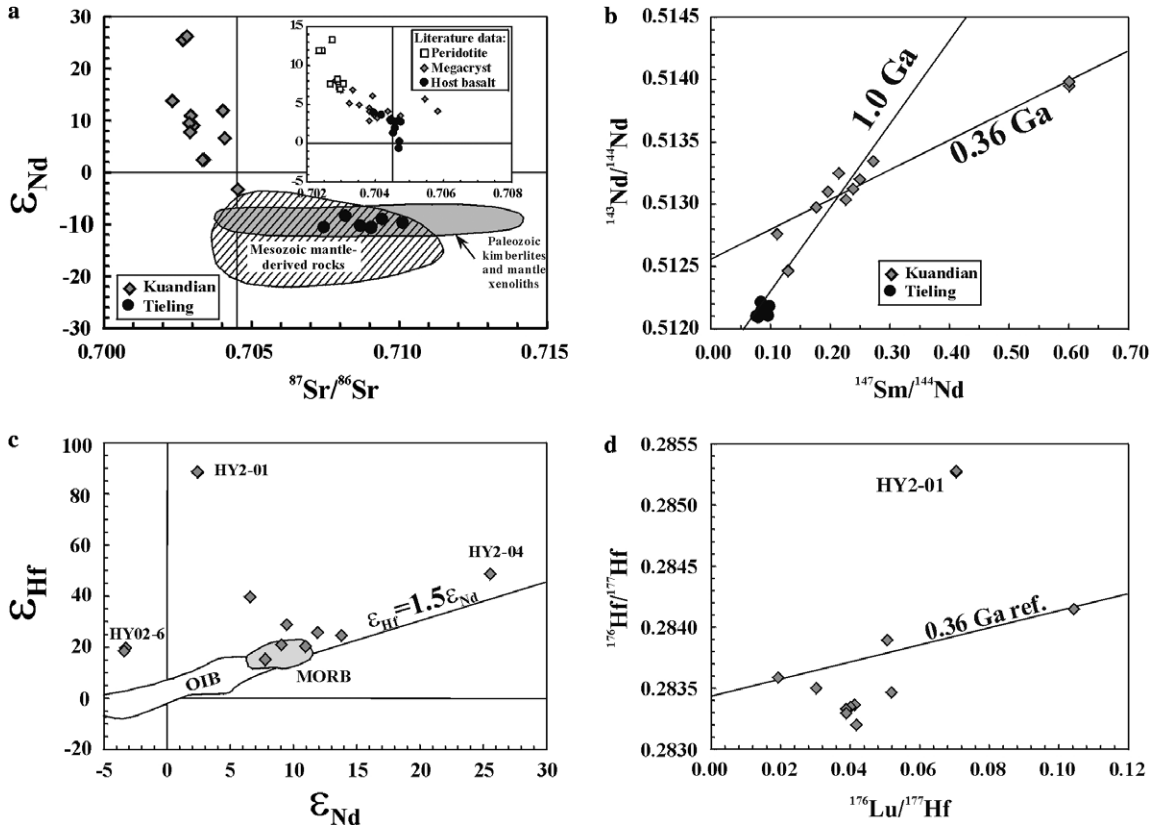


Fig. 6. Sr–Nd–Hf isotopic compositions of the clinopyroxenes from the Kuandian peridotites. Data sources in (a): Mesozoic mantle-derived igneous rocks (Guo et al., 2001, 2003; Chen et al., 2003, 2004; Zhang et al., 2003, 2004; Xu et al., 2004); Paleozoic kimberlites and their mantle xenoliths (Chi and Lu, 1996; Zheng, 1999); Literature data on Kuandian basalts, peridotites and megacrysts (Liu CQ et al., 1992; Tatsumoto et al., 1992; Xu et al., 1998).

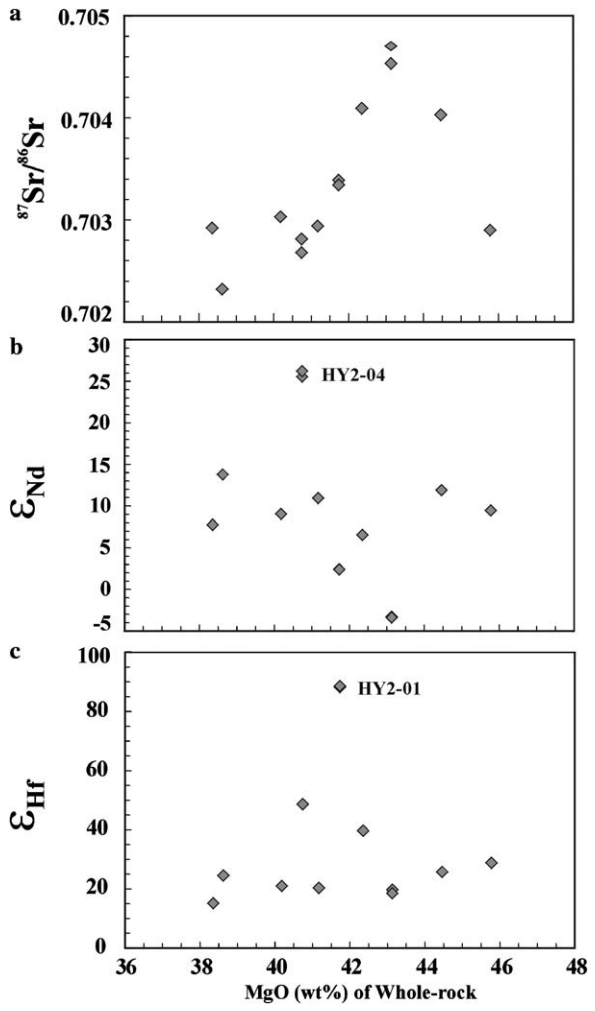


Fig. 7. Sr–Nd–Hf isotopic variations of clinopyroxenes versus MgO (wt%) of the Kuandian peridotites.

samples have had minimal *in situ* accumulation of $^{187}Os$ since eruption in their host lava.

As is common for peridotite xenolith suites from SCLM, the $^{187}Re/^{188}Os$ ratios do not correlate well with their $^{187}Os/^{188}Os$ ratios, although there is a crude positive correlation between the two parameters (Fig. 8a). The lack of a well-defined isochron can be attributed to several factors including the likelihood of derivation of samples from isotopically and chronologically distinct portions of the SCLM, and the possibility of late-stage Re mobility during transport to the surface (e.g. Chesley et al., 1999; Meisel et al., 2001). It is important to note, however, that the most refractory samples have lower $^{187}Re/^{188}Os$ ratios than those of the fertile lherzolites (Fig. 8b and c), suggesting that later-stage metasomatic alteration evident in the lithophile trace elements likely did not result in a substantial increase in Re abundances.

Osmium isotopic composition versus 1/Os and Cr# of spinel variation diagrams indicate that the Kuandian peridotites may have been derived from at least two distinct mantle sources (Fig. 8c). In the variation diagram of whole rock $^{187}Os/^{188}Os$ versus Cr# ([100Cr/(Cr + Al)]) of spinel (inserted in Fig. 8c), the samples can be divided into two subgroups; one with relatively high $^{187}Os/^{188}Os$ ratios of 0.1229–0.1275 and generally lower Cr#, and the other with lower $^{187}Os/^{188}Os$ ratios of 0.1137–0.1189 and generally higher Cr# (Fig. 8c). In the subgroup with the higher $^{187}Os/^{188}Os$ the most fertile samples, HY2-07 and HY2-29, have the highest $^{187}Re/^{188}Os$ and $^{187}Os/^{188}Os$ ratios of 0.33 and 0.51, and 0.1274 and 0.1269, respectively. The remaining five peridotites in this subgroup have compositions that are of intermediate fertility and have $^{187}Os/^{188}Os$ ratios of 0.1228 to 0.1271. Of note, clinopyroxene from sample HY2-04 has the most radiogenic Hf and Nd isotopic compositions of this suite ($\varepsilon_{Hf} = +48.7$; $\varepsilon_{Nd} = +26$), indicative of long term depletions in Lu relative to Hf and Nd relative to Sm. This is consistent with ancient removal of LREE-enriched melt from this rock. A prior history of melt depletion is also consistent with the low $^{187}Re/^{188}Os$ 0.082 in the bulk sample. However, the present day chondritic $^{187}Os/^{188}Os$ ratio of 0.1271 is inconsistent with a long-term depletion in Re/Os. This sample also has an unusually low Os concentration of 0.694 ppb. Combined, the relatively high $^{187}Os/^{188}Os$ and low Os concentration of this sample may reflect a late-stage metasomatic replacement of Os with more radiogenic Os.

Except for sample FW04-354, the peridotite xenoliths in the Tieling kimberlite are characterized by relatively high Os concentrations of 3.34–5.08 ppb and low Re concentrations of 0.010–0.035 ppb (Table 2). Their $^{187}Os/^{188}Os$ ratios range from 0.1112 to 0.1156. All samples have substantially sub-chondritic $^{187}Re/^{188}Os$ ratios of 0.009 to 0.045 (Fig. 8a). Therefore, these xenoliths were likely derived from a refractory mantle source with minimal *in situ* accumulation of $^{187}Os$ since their removal to the surface during the early Paleozoic. As noted above, sample FW04-354 has a much higher CaO content than other samples and may have been an olivine-pyroxenite. The much lower Os concentration of this sample (0.097 ppb), comparatively high $^{187}Re/^{188}Os$ (0.537) and much more radiogenic $^{187}Os/^{188}Os$ ratio (0.184) is consistent with this conclusion. Despite strong evidence for metasomatic enrichment in the lithophile trace elements (including Sr and Nd isotopes), the low Re/Os ratios and relatively high Os concentrations suggest that the metasomatic event had little impact on Re–Os systematics.

The chromites from the Paleozoic Fuxian, Mengyin and Tieling kimberlites have variable Re (0.05–0.62 ppb) and Os (1.00–6.01 ppb) concentrations. The Re concentrations are generally higher and the Os concentrations are generally lower than are typically found in chromites present in mafic–ultramafic systems (e.g. Walker and Stone, 2001; Walker et al., 2002). The chromites have variable $^{187}Re/^{188}Os$ ratios of 0.05–0.62 that overlap with the range determined for the Kuandian bulk samples (Fig. 8a). To our knowledge, however, Re–Os data for chromites separated from kimberlites have not previously been reported. The $^{187}Os/^{188}Os$ ratios from all three locations range narrowly from 0.1178 to 0.1124 (Fig. 8a).

Table 2
Re-Os isotopic and composition data for peridotites and chromites from Kuandian, Tieling, Fuxian and Mengyin

| Sample No. | Location | t (Ma) | MgO (wt%) | $Al_2O_3$ (wt%) | Fo (Olivine) | Cr# (Spinel) | T °C | Re (ppb) | Os (ppb) | $^{187}Re/^{188}Os$ | $^{187}Os/^{188}Os$ | $\gamma_{Os(t)}$ | $T_{RD}$ (Ga) | $T_{MA}$ (Ga) |
|---|---|---|---|---|---|---|---|---|---|---|---|---|---|---|
| *Peridotite xenoliths in Cenozoic basalts* | | | | | | | | | | | | | | |
| HY1-01 | Kuandian | 0 | 44.46 | 1.58 | 91.67 | 34.24 | 991 | 0.027 | 2.529 | 0.051 | 0.11712 | −7.8 | 1.46 | 1.67 |
| HY2-01 | Kuandian | 0 | 41.73 | 2.15 | 91.16 | 27.46 | 966 | 0.057 | 2.783 | 0.098 | 0.12296 | −3.2 | 0.60 | 0.79 |
| HY2-02 | Kuandian | 0 | 40.18 | 3.09 | 90.75 | 11.63 | 1027 | 0.017 | 0.884 | 0.094 | 0.12684 | −0.1 | 0.02 | 0.03 |
| HY2-03 | Kuandian | 0 | 41.17 | 3.08 | 90.57 | 13.32 | 840 | 0.097 | 2.192 | 0.214 | 0.12488 | −1.7 | 0.32 | 0.67 |
| HY2-04 | Kuandian | 0 | 40.74 | 2.56 | 90.22 | 11.93 | 925 | 0.012 | 0.692 | 0.082 | 0.12707 | 0.1 | −0.01 | −0.01 |
| HY2-05 | Kuandian | 0 | 45.78 | 1.19 | 91.79 | 39.69 | 973 | 0.045 | 1.751 | 0.124 | 0.11362 | −10.5 | 1.97 | 2.82 |
| HY2-06 | Kuandian | 0 | 43.13 | 2.55 | 90.72 | 17.57 | 807 | 0.020 | 2.217 | 0.043 | 0.11888 | −6.4 | 1.20 | 1.34 |
| HY2-07 | Kuandian | 0 | 38.35 | 4.06 | 90.34 | 11.40 | 1150 | 0.072 | 1.055 | 0.330 | 0.12740 | 0.3 | −0.06 | −0.33 |
| HY2-14 | Kuandian | 0 | 42.35 | 2.57 | 91.01 | 23.77 | 1055 | 0.017 | 1.518 | 0.055 | 0.12283 | −3.3 | 0.62 | 0.72 |
| HY2-29 | Kuandian | 0 | 38.62 | 4.26 | 90.04 | 9.88 | 1038 | 0.209 | 1.984 | 0.508 | 0.12686 | −0.1 | 0.02 | −0.08 |
| *Peridotite xenoliths in Paleozoic kimberlites* | | | | | | | | | | | | | | |
| FW04-350 | Tieling | 460 | | 1.11 | | | | 0.022 | 4.169 | 0.025 | 0.11123 | −10.4 | 2.34 | 2.46 |
| FW04-351 | Tieling | 460 | | 0.73 | | | | 0.011 | 4.646 | 0.011 | 0.11124 | −10.3 | 2.32 | 2.37 |
| FW04-352 | Tieling | 460 | | 1.36 | | | | 0.035 | 4.347 | 0.039 | 0.11263 | −9.3 | 2.15 | 2.32 |
| FW04-353 | Tieling | 460 | | 1.49 | | | | 0.010 | 4.205 | 0.012 | 0.11558 | −6.8 | 1.69 | 1.73 |
| FW04-354 | Tieling | 460 | | 0.76 | | | | 0.011 | 0.097 | 0.537 | 0.18390 | 45.1 | −8.45 | 21.1 |
| FW04-355 | Tieling | 460 | | 1.63 | | | | 0.031 | 3.336 | 0.045 | 0.11452 | −7.9 | 1.88 | 2.06 |
| FW04-356 | Tieling | 460 | | 0.91 | | | | 0.010 | 5.071 | 0.009 | 0.11128 | −10.3 | 2.31 | 2.35 |
| *Chromites in Paleozoic kimberlites* | | | | | | | | | | | | | | |
| FX-2 | Fuxian | 460 | | | | | | 0.054 | 1.000 | 0.258 | 0.11782 | −6.5 | 1.65 | 3.72 |
| FX-3 | Fuxian | 460 | | | | | | 0.120 | 4.942 | 0.117 | 0.11734 | −6.0 | 1.56 | 2.00 |
| FX-4 | Fuxian | 460 | | | | | | 0.084 | 1.847 | 0.219 | 0.11668 | −7.2 | 1.77 | 3.29 |
| MY-06 | Mengyin | 460 | | | | | | 0.618 | 6.008 | 0.494 | 0.11235 | −12.4 | 2.69 | −10.3 |
| FW04-347 | Tieling | 460 | | | | | | 0.100 | 2.170 | 0.223 | 0.11666 | −7.2 | 1.77 | 3.37 |

Note: (1) all the reported values have been corrected for mass fractionation and; (2) the parameters used in calculation are: $\lambda_{Re} = 1.666 \times 10^{-11}$/year $(^{187}Re/^{188}Os)_{Chond} = 0.40186$, $(^{187}Os/^{188}Os)_{Chond,0} = 0.1270$ (Shirey and Walker, 1998); (3) T °C is calculated according to Kohler and Brey (1990).

## 6. Discussion

### 6.1. Petrogeneisis of the Kuandian peridotite xenoliths

The Kuandian peridotites are residues of variable extents of partial melting of the mantle in the spinel field. The xenoliths contain no garnet, so they probably originated from mantle source depths of less than ~80 km, based on estimates of the spinel-garnet transition (Klemme and O'Neill, 2000). After the original partial melting event(s), the clinopyroxene-poor lherzolites and the harzburgites underwent metasomatic alteration, as evidenced by enrichments of incompatible lithophile elements (Figs. 3 and 5).

The nature of metasomatic agents involved in the alteration of SCLM, in general, has been highly debated (Meen et al., 1989; Bodinier et al., 1990; Ionov et al., 1997; Downes, 2001; Pearson et al., 2003). Possible metasomatic agents include water, $CO_2$, and carbonatitic and silicate melts. Yaxley et al. (1998) suggested that carbonatite metasomatism of SCLM leads to a reduction in the Ti/Eu of bulk peridotites, whereas this ratio normally remains unchanged at ~8000 by variable degrees of partial melting. Most Kuandian xenoliths have Ti/Eu ratios between 8700 and 11900 with only two samples having low ratios of 2970 and 4900, hence carbonatite metasomatism can be ruled out.

The presence of amphibole in one sample (HY2-06), coupled with strong enrichments in incompatible trace elements indicates that aqueous metasomatism affected at least one of the samples. Either aqueous or silicate melt metasomatic transport of incompatible elements could have had a major impact on Sr–Nd–Hf isotopic systematics of these rocks, hence, mineral and whole rock compositions may not reflect the isotopic systematics of the pre-metasomatized mantle. The negative trend for $\varepsilon_{Nd}$ versus $^{87}Sr/^{86}Sr$ (Fig. 6a) and the relatively low $\varepsilon_{Hf}$ value of some samples is consistent with the variable addition of Sr, Nd, and Hf from a source with long-term enrichment in Rb/Sr, Nd/Sm, and Hf/Lu, to a long-term variably melt depleted source. Although aqueous transport can evidently lead to the transport and deposition of Os, particularly in supra-subduction zone mantle, such transport is also normally accompanied by net loss of Os, e.g. low Os concentrations in peridotitic rocks (e.g. Brandon et al., 1996). For the Kuandian suite, the two samples (HY2-04 and HY2-07) with the highest $^{187}Os/^{188}Os$ ratios of ~0.127 have the lowest Os concentrations within the suite, 0.69 and 1.1 ppb, which may implicate aqueous addition of Os with high $^{187}Os/^{188}Os$ to these rocks. However, it should be noted that the amphibole-bearing sample HY2-06 has a substantially higher Os concentration (2.2 ppb) and lower $^{187}Os/^{188}Os$ (0.119).

### 6.2. Petrogenesis of the Tieling peridotite xenoliths

Due to the alteration and a paucity of primary minerals, *P–T* conditions of the Tieling peridotites can not be well constrained at present. Chi and Lu (1996) reported the

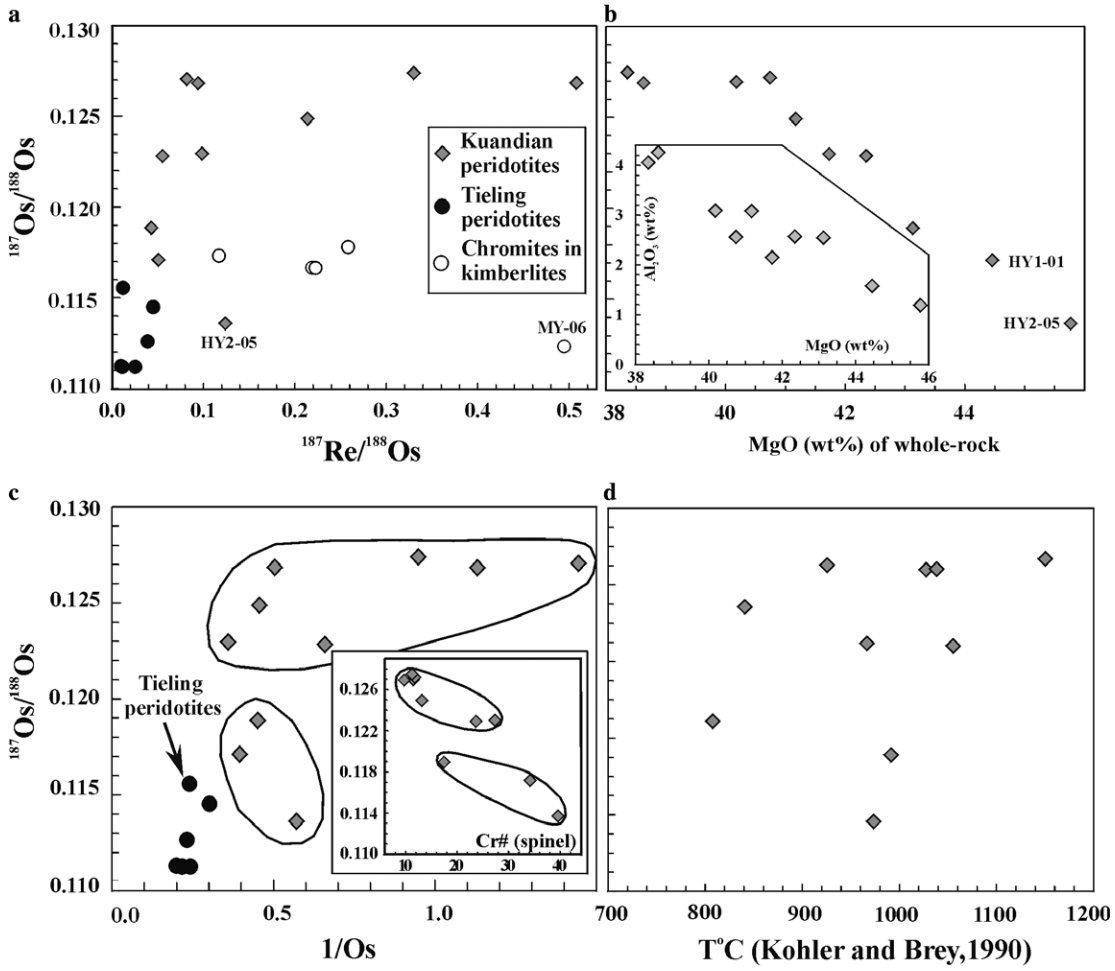


Fig. 8. Os isotopic compositions and variations of the peridotite xenoliths in Kuandian. The Os isotopic ratios correlate well with the melt depletion degree shown by MgO (wt%) of whole-rock (a) and Cr# number of spinel (b). In the Re–Os variation diagram, no isochron could be yielded although there is no Re addition after formation (c). (d) Plots of equilibrium temperature (Brey and Kohler, 1990) against Os isotopic composition, indicating the complex vertical age structure for the SCLM in the Kuandian area.

presence of garnet in mantle xenoliths from neighboring kimberlite pipes. Only spinel, however, has been observed in the samples studied here, suggesting minimum derivation depths of ~80 km, similar to those of the Kuandian xenoliths. Further petrological and mineralogical studies will be required to more firmly constrain depth of origin and original compositions.

The residual mineral assemblage after alteration indicates that the Tieling peridotites originated as harzburgites. This assumption is also supported by their low concentrations of $Al_2O_3$, suggesting that these xenoliths were the residue of a higher degree of partial melting than those from Kuandian. However, the very LREE enriched nature of the rocks, especially given the depleted major element compositions suggest an initial melt depletion event, followed after some time by an event that transported incompatible trace elements into the peridotite. Sample FW04-354 has a high Ca content and was originally probably a pyroxenite. Sr–Nd results are all consistent with the metasomatic addition of materials with long-term enrichments in Rb/Sr and Nd/Sm, characteristics that are considerably different (particularly higher Rb/Sr) from that in the Kuandian xenoliths.

### *6.3. Paleozoic SCLM age constrained by peridotites and chromites in kimberlites*

Gao et al. (2002a) reported Archean Os model melt depletion ages for two xenoliths erupted from an early Paleozoic kimberlite pipe at Fuxian. One highly refractory sample from another early Paleozoic kimberlite at Mengyin, approximately 500 km to the southwest of Fuxian, in contrast, had a younger $T_{RD}$ age of 1.4 Ga (Gao et al., 2002a). The Mengyin bulk sample, however, had a relatively high Re/Os, so if that ratio was substantially greater than zero during the evolution in the mantle, the melt depletion age could have been considerably older and more similar to the Fuxian results.

Accumulation of more melt-depletion age information for mantle xenoliths from these and other Paleozoic volcanic centers is critical to deciphering the evolution of the SCLM underlying the NCC. However, peridotite xenoliths

of suitable size for analysis at Fuxian and Mengyin are rare. Chromite megacrysts are an alternate material to study that may give complementary age information to peridotite xenoliths, and we analyzed four from these two locales for this study. Chromites are highly resistant to alteration, and chromites from mafic–ultramafic intrusions and ophiolites typically have the desirable features of low Re concentrations, high Os concentrations, and very low Re/Os ratios. Also, the Re/Os ratios of chromites may be more representative of compositions at eruption, or even mantle compositions than those of bulk samples. Rhenium is likely located in sulfides that are shielded within the alteration resistant chromite. Dispersed sulfides in bulk samples are much more easily modified by melt contamination and surface weathering processes.

There have been numerous mineralogical studies of the compositions of chromites from the Mengyin and Fuxian kimberlites (Dobbs et al., 1994; Bao et al., 1995; Chi and Lu, 1996; Zhao, 1998; Zheng, 1999). It has been concluded that chromites from Mengyin probably did not form as phenocrysts in the kimberlitic magmas, but instead are xenocrysts disaggregated from garnet peridotites, and may thus be direct samples of SCLM (Dobbs et al., 1994; Chi and Lu, 1996; Zheng, 1999). The one chromite analyzed from Mengyin (MY-06) has the highest Os concentration (6.01 ppb) among the analyzed chromites, and has a $^{187}Os/^{188}Os$ ratio of 0.1124. The chromite has a suprachondritic $^{187}Re/^{188}Os$ ratio of 0.494. If it is assumed that the Re/Os reflects the composition since eruption at 460 Ma, this sample has a calculated $^{187}Os/^{188}Os$ ratio of 0.1085 at the time of eruption, consistent with a $T_{RD}$ age of ~2.7 Ga. This indicates that mantle with Archean melt depletion history was present in the SCLM underlying Mengyin during the early Paleozoic. The $T_{RD}$ of this sample contrasts with the bulk peridotite sample reported by Gao et al. (2002a), but as noted above, that sample may have a much older melt depletion history than reported.

The origin of chromites from Fuxian is more complex, and chromite macrocrysts evidently occur as both xenocrysts and phenocrysts (Bao et al., 1995; Chi and Lu, 1996; Zhao, 1998; Zheng, 1999). According to Zhao (1998), the mineral inclusions in chromites from the Fuxian kimberlite form four distinctive groups: silicates, carbonates, hydrous silicates, and sulfides. Mineral compositions and comparison of mineral inclusions relative to the same minerals in diamonds suggest that the inclusions of carbonates and silicates may represent kimberlitic magma that was trapped during kimberlite generation. These chromites likely formed as phenocrysts in the kimberlitic magmas. In contrast, chromites with sulfide inclusions were considered to be fragments of the SCLM. All three of the Fuxian chromites examined here were sulfide-bearing and are therefore likely xenocrysts. They have subchondritic $^{187}Re/^{188}Os$ and $T_{RD}$ ages ranging between 1.6 and 1.8 Ga. The model ages for the Fuxian chromites are, thus, younger than the Archean model ages reported for the Fuxian bulk peridotites (Gao et al., 2002a). It is possible that the Re present in these chromites was incorporated at the time of mineral formation and not eruption. If so, the chromites would have substantially older model ages. Model $T_{MA}$ ages range from 2.0 to 3.7 Ga.

The Tieling peridotite xenoliths are refractory, as indicated by their low $Al_2O_3$. Yet the LREE and other incompatible element enrichments indicate considerable modification subsequent to initial melting. Except for sample FW04-354, which has an unusually low Os content and high $^{187}Re/^{188}Os$ ratio, the remaining six samples have Os model $T_{RD}$ ages of 1.7–2.3 Ga, with most >2.1 Ga. On a plot of $Al_2O_3$ versus $^{187}Os/^{188}Os$ (Fig. 8a), regression of these data through PUM with extrapolation to $Al_2O_3$ of 0.7 wt% (Appendix A) gives a corresponding $^{187}Os/^{188}Os$ of ~0.110, consistent with a late Archean melt depletion event occurring at about 2.5 Ga (Fig. 8a). This provides strong evidence that the SCLM beneath Tieling, presumably during the early Paleozoic, included residue of Archean melting. This result is consistent with the Fuxian result of Gao et al. (2002a). No highly-depleted samples from Tieling have been found to have $^{187}Os/^{188}Os$ ratios comparable to estimates of the convecting upper mantle during the Paleozoic, so there may have been little Phanerozoic SCLM at that time. The model $T_{RD}$ age for a chromite megacryst from the Tieling kimberlite is 1.8 Ga, which is considerably younger than the model age of 2.5 Ga obtained by regression of the bulk peridotites. The $T_{Ma}$ age is considerably older (3.4 Ga). However, the origin of that particular chromite is less well constrained than the other chromites.

In summary, the combined data for materials derived from early Paleozoic volcanic systems in the eastern NCC, Mengyin, Fuxian, and Tieling (presumed to be early Paleozoic) provide strong evidence for the presence of SCLM with a dominant late Archean melt depletion history at the time of volcanism. The only evidence for potentially younger melt depletion comes from $T_{RD}$ ages obtained for some of the chromites. As noted, these data are difficult to interpret at the present time because it is not yet well defined how Re/Os is modified in mantle chromites post crystallization. If the chromites survived with the measured Re/Os from the time of formation, the Os model ages largely agree with bulk peridotite data. Alternately, the Fuxian results may indicate that SCLM with a Proterozoic melt depletion history also underlay the eastern portion of the NCC during the Paleozoic. There is no evidence in any of the suites for post 1.5 Ga SCLM, even though the absence of garnet in these samples suggests they were likely derived from relatively shallow portions (<80 km) of the thick SCLM present at that time. The implication is that if the SCLM was progressively accreted downward, younger materials may have been present at greater depths at that time, but are no longer present.

### 6.4. Age of SCLM beneath the North China Craton during the Cenozoic

The age and structure of the SCLM underlying the modern NCC is still currently debated (Griffin et al., 1998;

Menzies and Xu, 1998; Xu, 2001; Gao et al., 2002a; Wu et al., 2003). Previous studies have implicated mostly relatively young SCLM, but also with some evidence for materials with Paleo-through Neoproterozoic melt extraction. The new data are consistent with complexity in age structure. The two Kuandian harzburgites (HY1-01 and HY2-05) and the cpx-poor lherzolite (HY2-06) (Fig. 8b) have $T_{RD}$ model ages of 1.2–2.0 Ga, respectively. Although these samples are the most refractory of the suite, they both have >1 wt% $Al_2O_3$ and as such are not highly refractory. Consequently, the model $T_{RD}$ ages may significantly underestimate melt depletion ages (Appendix A). Lithophile trace element data for the more refractory xenoliths indicate moderate addition of incompatible elements via some form of metasomatism. This means that Re may also have been added and that the $T_{MA}$ ages of 1.3–2.8 Ga for these three rocks may also be problematic. Although the Kuandian xenoliths do not define a well-correlated linear trend, regression of the harzburgite data through the PUM composition, and extrapolation to 0.7 wt% $Al_2O_3$ gives a corresponding $^{187}Os/^{188}Os$ of ~0.1115, consistent with a model age of ~2.3 Ga, slightly younger than the Tieling peridotites (Fig. 9a). Six of the 10 samples plot relatively close to this line. This model age overlaps with, but is generally younger than the overlying crustal formation ages. It is consistent with melt depletion occurring during the Paleoproterozoic, and provides evidence for substantially older SCLM presently underlying the NCC than previously reported for Cenozoic volcanoes.

Despite the evidence for Paleoproterozoic melt depletion, seven of the more fertile Kuandian samples have $^{187}Os/^{188}Os$ ratios that are within the range of estimates for the modern convecting upper mantle, as defined by abyssal peridotites and ophiolites. This may indicate the presence of much younger additions to the SCLM in this region, and leads to the suggestion that the Kuandian suite provides evidence for at least two periods of melt extraction from the lithosperic mantle sampled. In a general sense, the evidence for generally young material is similar to the age structure at the Longgang and Qixia locales (Fig. 9a).

It remains unclear whether there is a correlation between model melt extraction ages and depth. Lack of garnet in the Kuandian suite is indicative of derivation from depths of <50 km, but no further depth resolution via pressure estimates can currently be achieved. The two xenoliths defining the late Paleoproterozoic trend have equilibration temperatures within the middle of the range defined by the suite (Fig. 8d), So there is no evidence to suggest that the peridotites with older melt extraction ages were derived from cooler, possibly shallower mantle than the samples with younger melt depletion ages.

The combined Os results for peridotites from three Cenozoic volcanic centers, Kuandian, Longgang, and Qixia, indicate that the present SCLM underlying the eastern portion of that NCC retains melt depletion ages for the Paleoproterozoic through to the Phanerozoic. The presence

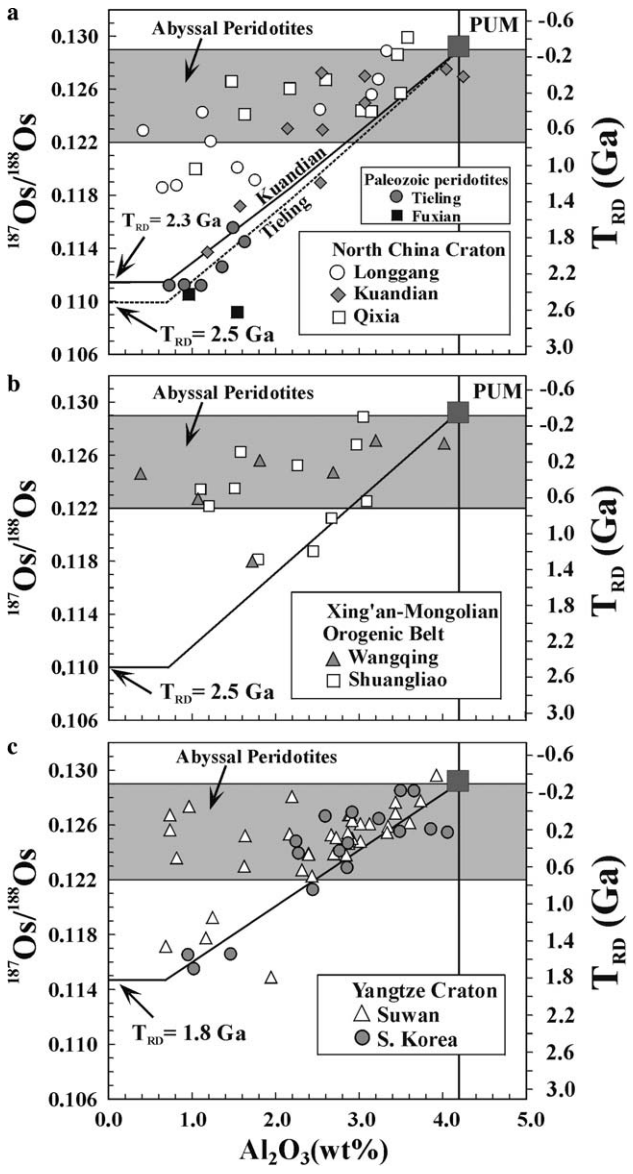


Fig. 9. Os isotopic composition versus $Al_2O_3$ (wt%) for different tectonic units in eastern China in Cenozoic. (a) The Xing'an-Mongolian Orogenic Belt (Wu et al., 2003), (b) North China Craton (Gao et al., 2002a; Wu et al., 2003) and (c) Yangtze Craton (Zhi et al., 2001; Zhi and Qin, 2004). The abyssal peridotite data are from Snow and Reisberg (1995) and Brandon et al. (2000). PUM- Primitive Upper Mantle (Meisel et al., 2001).

of samples that provide Os isotopic evidence for ancient melt depletion argues that if lithospheric delamination occurred, it did not uniformly remove all of the SCLM.

There is also some age information available for portions of the NCC to the west of the above locales (e.g. Hannuoba), and from adjoining cratons. In brief, the data for xenoliths sampled by Cenozoic volcanic rocks from Hannuoba indicate a replacement of Archean SCLM by new material added at about 1.9 Ga (Gao et al., 2002a), hence, potentially several 100 Ma younger than is suggested by the Kuandian xenoliths to the east. Osmium isotopic data for xenoliths derived from the Shuangliao and Wangqing volcanic systems in the Xing'an Mongolian Orogenic Belt to the north of the NCC, in the Suwan volcanic system from

the Subei basin, in the Yangze Craton to the south of the NCC, and the possible extensions of the NCC and Yangtze cratons to the east of the NCC, as exposed on the Korean peninsula, have recently been published (Wu et al., 2003; Zhi and Qin, 2004; Reisberg et al., 2005; Lee and Walker, 2006). The Os isotopic systematics of the xenoliths derived from these Cenozoic systems are similar to what is observed in the Cenozoic NCC (Fig. 9b and c). Three of the four suites (Suwan, Korea, Xing'an Mongolian Orogenic Belt) are dominated by materials with Phanerozoic melt depletion ages. A few samples from each locale, however, have more depleted $^{187}Os/^{188}Os$ and are consistent with Paleoproterozoic melt extraction, although samples with depleted $^{187}Os/^{188}Os$ have >1.5 wt% $Al_2O_3$, so the true ages of melt depletion are very poorly constrained. None of these locations bear xenoliths with evidence for Archean melt depletion. These combined results suggest that complexity in the age structure of the NCC extends to both the west, south and east of the locations considered here.

### 6.5. Constraints on the mechanism of lithospheric thinning beneath the NCC

One outcome of partial melting of the mantle that leads to the creation of continental crust may be the formation of residual SCLM that is buoyant and rigid, due its increased Mg and decreased water contents relative to the ambient convecting upper mantle (Jordan, 1988; Boyd, 1989; Walter, 2003). Accordingly, the crust and the SCLM "keel" may become mechanically and chemically coupled (Doin et al., 1997; Griffin et al., 1999a; Poudjom Djomani et al., 2001; O'Reilly et al., 2001; Sleep, 2005). Such a relation is consistent with the longevity of coupled crust and SCLM keels, as has been documented for the Kaapvaal craton (e.g. Walker et al., 1989).

The new data presented here buttress earlier observations that an Archean SCLM keel underlay the NCC during the early Paleozoic. However, Os isotopic data for Cenozoic SCLM xenoliths, coupled with geophysical evidence for thin lithosphere at present are consistent with subsequent loss of the Archean keel. So what mechanisms can lead to lithospheric thinning of this magnitude? At least two possible causes for lithospheric thinning have been previously proposed, either generically or specifically for the NCC, thermal-mechanical erosion and delimination. They are not mutually exclusive.

One possibility is that the thinning was accomplished by thermal-mechanical erosion of the original SCLM (Menzies and Xu, 1998; Griffin et al., 1998; Xu, 2001; Xu et al., 2004; Zheng et al., 2001; Guo et al., 2003; Zhang, 2005). This can occur by injection of hot material, possibly via an upwelling plume. The added heat can cause melting and subsequent melt removal, resulting in a thinning of lithospheric mantle. This process must result in transfer of mass from the mantle to the crust to achieve thinning.

A second possibility is delamination, the physical removal via foundering of lithospheric materials as a coherent mass (Wu and Sun, 1999; Wu et al., 2000, 2003; Gao et al., 2002a, 2004). This concept is based on the conclusion that chemical buoyancy and high viscosity are ineffective mechanisms for retaining lithospheric coherence if a craton becomes juxtaposed with a subduction zone, or a craton becomes tectonically active through plate collision (Bird, 1979; Pysklywec et al., 2000; Beck and Zandt, 2002; Lenardic et al., 2003). In such cases, the lithospheric mantle is no longer viscous and can be deformed. Crustal thickening may result from the transformation of mafic rocks in the lower crust into eclogite, which would then delaminate due to an increase in density (Gao et al., 2004). During and after delamination, crustal melting induced by upwelling of the hot asthenosphere could remove less dense material from the lower crust, potentially leaving behind more dense material that could also delaminate from the upper crust.

For the NCC, there are arguments against both possible end-member processes. Arguments against thermal erosion include: (1) the assumption that thermal erosion is initiated by the presence of a mantle plume that is hotter than the ambient surrounding mantle (Yuen and Fleitout, 1985; Davies, 1994). There is, however, no evidence for a Mesozoic-Cenozoic plume impacting the NCC; (2) thermal erosion would likely elevate the lithospheric-asthenospheric boundary, leading to further melting in the mantle lithosphere and potentially bias the residual SCLM to clinopyroxene-poor harzburgite. However, the Cenozoic SCLM accessed by volcanoes is dominated by clinopyroxene-rich lherzolite. Harzburgites are rarely found in the NCC; (3) thermal processes cannot explain the presence of high-Mg basalts, andesites and dacites identified by Gao et al. (2004) and the presently evolved composition and slow seismic velocities of the NCC crust (particularly the lower crust) compared to the global continental crust (Gao et al., 1992, 1998); (4) the eastern NCC experienced magmatism over a long period (~100 Ma). At face value, this seems to favor the erosion model. However, compilation of recent data suggests that instead, the magmatism occurred largely during two peaks at 195–150 and 130–120 Ma, rather than a gradual, long-lived event (Wu et al., 2005a,b).

Arguments against delamination include: (1) there may be an insufficient density difference between the cratonic SCLM and underlying asthenospheric mantle for delamination to occur (Xu et al., 2004); (2) some models suggest that delamination would most likely be a short term process and the resulting influx of hotter mantle would likely lead to intensive crustal melting (Kay and Kay, 1993; Lustrino, 2005). In contrast, the duration of Mesozoic and Cenozoic magmatism in the NCC extended for more than 100 Ma (Xu et al., 2004); (3) delamination of the lower lithosphere would result in upwelling of the convective mantle, which would in turn result in large scale decompression melting and the production of voluminous basalts.

The petrology of the NCC xenoliths, combined with new and previously published Os isotopic data for NCC peridotite xenoliths and kimberlite chromites pose prob-

lems for both the thermal-mechanical erosion and the delamination models. An Archean keel to the NCC appears to have been removed as a consequence of thinning, but the residual or replacement lithopheric mantle appears to be of variable age. Consequently, a key issue to resolve regarding this conundrum is the reason for the presence of lithospheric mantle with apparent Proterozoic melt depletion ages sampled by xenoliths derived from Cenozoic volcanic systems.

We consider three possibilities for the survival of Proterozoic materials in the SCLM underlying the NCC: (1) stratigraphic variations in melt depletion ages such that removal of Archean SCLM could leave behind Proterozoic and younger SCLM, (2) geographic variations in the age structure of SCLM such that the thinning event removed Archean through Phanerozoic materials in the underlying SCLM, leaving behind materials of all ages, but with Cenozoic volcanism only accessing Proterozoic or younger materials, or (3) replacement of Archean SCLM during the thinning event with Proterozoic through Phanerozoic age lithospheric mantle that formed elsewhere.

Given the still limited data for xenoliths from Paleozoic volcanic systems, it is possible that Archean SCLM that was present prior to thinning was overlain by materials with Proterozoic melt depletion ages. Removal of the deeper materials with Archean melt depletion history could then have left behind the younger, Proterozoic materials. An inverted age stratigraphy in SCLM, however, has not previously been observed. Instead, the age structure of SCLM is often characterized by having no resolvable age variation with depth, such as for the SCLM underlying the Kaapvaal, South Africa and Siberian cratons (e.g. Carlson et al., 2000, 2005; Pearson et al., 2003), or younging with increasing depth, such as for the SCLM underlying Tanzania, and the Slave and Wyoming cratons (Carlson et al., 1994, 1999; Chesley et al., 1999; Griffin et al., 1999b; Kopylova and Russell, 2000; Irvine et al., 2003; Aulbach et al., 2004). In these cases, SCLM evidently grew within a relatively short time interval, or by gradual accretion downward.

It is conceivable that SCLM with Proterozic melt depletion ages could overlie Archean SCLM for a scenario where SCLM melting at greater depths contributed to the construction of the overlying continental crust, but relatively fertile mantle remained at shallower depths. In such a case, a subsequent thermal event, such as the imposition of a plume, could result in the partial melting of the more fertile materials at shallower depths. This material would not be younger than the underlying materials with Archean melt depletion ages, but would record a younger melt depletion age because this would be the first event leading to Re removal in these rocks. This hypothesis would be strengthened if materials derived from shallow levels of the SCLM with bona fide Proterozoic model melt extraction ages are eventually discovered in the Paleozoic kimberlites. The Mengyin bulk sample reported by Gao et al. (2002a), and the Fuxian and Tieling chromite data presented here may be consistent with this, but these data are insufficiently robust for the reasons discussed above to currently make a strong conclusion.

The fact that the Fuxian xenoliths and xenoliths similar to those from Tieling contain garnet is consistent with their derivation from relatively deep SCLM. If an inverted age stratigraphy existed in the SCLM during the time of Paleozoic volcanism, the present age structure could be explained via partial delamination of the lithospheric mantle. The greatest weakness of this model, however, is that it cannot solely account the presence of highly-depleted xenoliths in Cenozoic volcanic systems with Os isotopic compositions consistent with the modern convecting upper mantle.

It is also possible that the age structure of the SCLM underlying the NCC may vary with geographic location. This could reflect localized destruction of the Archean materials as a consequence of cratonization and tectonization events during the Proterozoic, resulting in the melting of fusible mantle at these times. For example, assemblage of at least some of the blocks comprising the NCC occurred during the Paleoproterozoic, so some of the rocks with evidence for Proterozoic melt depletion may have formed as a result of partial melting of relatively shallow SCLM that could be associated with addition of new mantle at that time, or was mantle that had not been previously melted (Zheng et al., 2004; Wu et al., 2005a). For this model, it would be expected that Proterozoic SCLM underlies former sutures and that the sites of Cenozoic volcanism should reflect suture locations. The lithospheric thinning would then have removed both Archean and Proterozoic SCLM. As with the previous model, this model alone cannot account for the presence of younger materials in the Cenozoic SCLM. Also, there does not appear to be a correlation between the locations of former sutures and the Cenozoic volcanic centers.

Finally, there is evidence to suggest that mantle underlying collision zones of major continental crustal blocks can be extruded away from the collision and thrust under other crustal blocks (e.g. Tapponnier et al., 1982; Fouch, 2000). For example, it has been suggested that ancient SLCM originally underlying India and Asia has been extruded away from the India-Asia collision zone and may now underlie parts of southeast Asia (Xu et al., 2001; Flesch et al., 2005). This type of mechanism can potentially lead to the emplacement of either younger or older lithospheric mantle materials under a continental crustal block. Indeed, several studies have documented crust-lithospheric mantle age relations where the mantle is either younger or older than the overlying crust, such as in the Mojavia of the US Basin and Range province, the Canadian Cordillera and eastern Australia (Lee et al., 2000, 2001; Peslier et al., 2000a; Handler et al., 2005).

The NCC experienced at least three major tectonic events during the Phanerozoic, the Permian collision of the accretionary complexes in the Central Asian Orogenic Belt in north, the Triassic collision of the Yangtze Craton in south, and the Mesozoic-Cenozoic subduction of the

Pacific plate in east. The northward subduction of the Yangtze Craton beneath the NCC resulted in the formation of the Dabie-Sulu ultrahigh-pressure metamorphic belt (Hacker et al., 1998). Exsolution of clinopyroxene, rutile and apatite in eclogites from Yangkou in the Sulu ultrahigh-pressure metamorphic belt suggests possible subduction of continental materials to depths greater than 200 km (Ye et al., 2000). Therefore, the Proterozoic SCLM underlying the NCC could have formed as SCLM underlying the Yangtze Craton, that was underthrust or extruded under portions of the NCC resulting from collision. This event may have precipitated the thinning event, or thinning may have occurred subsequently, induced by the NNW subduction of the Pacific plate under the NCC during the late Mesozoic.

## 7. Summary

New data for peridotite xenoliths sampled by Paleozoic and Cenozoic volcanic systems are consistent with previous studies in confirming a dominantly Archean melt depletion signature in the SCLM underlying the NCC during the early Paleozoic, but a Paleoproterozic through Phanerozoic signature during the Cenozoic. The peridotites from Cenozoic Kuandian basalts are characterized by low $^{87}Sr/^{86}Sr$, high $\varepsilon_{Nd}$ and $\varepsilon_{Hf}$ values, indicating their derivation from long-term depleted mantle. A trend towards higher $^{87}Sr/^{86}Sr$, lower $\varepsilon_{Nd}$ and lower $\varepsilon_{Hf}$ values indicates a modification of these rocks via interactions with recycled crustal materials. In contrast, the Tieling peridotites found in Paleozoic kimberlites are extremely enriched in incompatible trace elements and are characterized by relatively high $^{87}Sr/^{86}Sr$, and low $\varepsilon_{Nd}$ and $\varepsilon_{Hf}$ values. The chronological and elemental data indicate a major change in the composition of the SCLM underlying the NCC, likely corresponding with the lithospheric thinning event that is evidenced through petrologic and geophysical observations.

The mechanism causing the thinning remains elusive. Although thermal mechanical erosion and delamination can account for the thinning, either alternative requires a relatively complex sequence of events to result in the apparent complex age structure now present under the NCC. To resolve the true causes of lithospheric thinning and the resulting chronologic complexity of the resident SCLM, additional data for materials from the SCLM covering a broader geographic range than is presently available, and additional data for mantle materials sampled by Paleozoic volcanic systems will likely be required.

## Acknowledgments

This work was supported by grants (40325006 and 40133020) from the National Natural Science Foundation of China (to F.Y.W.) and National Science Foundation Grant EAR 9909197 (to R.J.W.). F.Y.W. acknowledges the hospitality of the Isotope Geochemistry Laboratory during his visit to Maryland (May of 2005). S.R. Lee and I. Puchtel are thanked for their help during the chemical separation and mass spectrometric analyses. R.L. Rudnick read an early version of the manuscript, and gave invaluable suggestions. We thank A. Peslier, S. Gao and an anonymous reviewer for their comprehensive and constructive comments. M. Menzies is thanked for editorial assistance and an additional constructive review.

*Associate editor:* Martin A. Menzies

## Appendix A. Considerations of the Re–Os isotope system for dating mantle melt depletion

The placement of age constraints is critical to deciphering the formation and modification history of the SCLM underlying the NCC. As previously discussed, the Sr, Nd, and Hf isotopic systematics of the xenoliths were evidently variably affected by metasomatic events, so do not likely record ages of primary melting. Consequently, for age constraints we largely rely on the Re–Os isotope system. Although commonly used for this purpose, it is important to briefly review the assumptions and complexities involved in its application.

The Re-Os isotopic system ($^{187}Re \rightarrow {}^{187}Os + \beta^-$; $\lambda = 1.67 \times 10^{-11} yr^{-1}$) serves as a potentially effective chronometer for the formation of residues of partial melting of the mantle. The system differs from other long-lived radiogenic isotope systems in that the daughter element Os is highly compatible with mantle residues while the parent element Re is incompatible during mantle melting (Walker et al., 1989). Removal of Re with melt effectively leads to retardation or cessation in the growth of $^{187}Os$. Because of the lack of the parent isotope, the system becomes relatively immune to subsequent diffusive resetting at high temperatures in mantle peridotites. As noted above, with certain exceptions (Brandon et al., 1996, 1999; Peslier et al., 2000b), the system is also resistant to metasomatic alteration due to the relatively high Os concentration of residual mantle.

Osmium model ages for mantle residues can be derived by several methods. Time of Re depletion ($T_{RD}$) model ages can provide constraints on the minimum ages of mantle melt depletion (Walker et al., 1989; Shirey and Walker, 1998). $T_{RD}$ model ages are calculated by assuming that a single melting event removes all of the Re from a peridotite, effectively freezing-in the isotopic composition of mantle evolving along a chondritic path prior to that time (Walker et al., 1989). For peridotites transported to the surface by non-zero age volcanic systems, the $^{187}Os/^{188}Os$ ratio of the sample at the time of eruption is normally calculated from its present isotopic composition and $^{187}Re/^{188}Os$. $T_{RD}$ ages will significantly underestimate the age of a melt depletion event for samples that have experienced only partial Re removal, such as in the case of lower extents of partial melting. However, as melting degree increases, the Re/Os ratio of the residuum approaches zero, and $T_{RD}$ may approach the true time of melt depletion. Therefore, $T_{RD}$ ages are applicable for only very highly refractory peridotites (e.g. $Al_2O_3 \leqslant 1.2$ wt%).

Peridotites that have undergone only modest melt depletion may retain substantial Re. For such samples, model $T_{MA}$ ages may be more accurate (Shirey and Walker, 1998). They are calculated based on measured $^{187}Re/^{188}Os$, and record the intersection of the isotopic evolution of a sample with a mantle evolution model. The accuracy of $T_{MA}$ model ages may be compromised by Re addition or loss during the history of the rock, but especially in transit to the surface in typically high Re volcanic systems.

Both $T_{RD}$ and $T_{MA}$ model age calculations are subject to further uncertainties. Three issues are noted. First, it has been observed that sulfides and alloys within some individual mantle peridotites may record different periods of melt depletion (Alard et al., 2002, 2005). Some sulfides may even have suprachondritic $^{187}Os/^{188}Os$ reflecting metasomatic enrichment resulting from the introduction of Os from a source with long-term high Re/Os. Thus, Os analyses of some bulk peridotites may record an averaged depletion history that does not reflect the age of an actual event (Alard et al., 2002). This normally would bias model age estimates, based on analyses of bulk samples, to younger ages than the true depletion age. Consequently, it can normally be assumed that samples with Archean model ages are dominated by Archean melt depletion.

Second, it is clear that the DMM is not isotopically homogeneous with respect to Os, and that even young DMM includes peridotites with old (in some cases Archean) melt depletion histories (e.g. Brandon et al., 2000; Reisberg et al., 2004). Materials with such ancient provenance appear to be relatively minor components of the DMM, so while a single sample with a depleted Os isotopic composition is not strong evidence for the presence of ancient SCLM, several studies suggest that random sampling of the convecting upper mantle would be dominated by materials with the average upper mantle isotopic composition (e.g. Meibom et al., 2002).

Third, the average Os isotopic composition of the modern DMM is still poorly known, so the mantle evolution model with which to compare the compositions of peridotites can vary by several percent at present (e.g. Snow and Reisberg, 1995; Brandon et al., 2000; Walker et al., 2002; Harvey et al., 2006). This means that Os model age determinations for peridotites with melt depletion ages less than about 1 Ga are very poorly constrained. Consequently, the resolution for dating SCLM melting events during the Phanerozoic is very poor. This is much less of a problem for older systems because possible variance from chondritic evolution was less in the past.

Another way to consider melt depletion ages of suites of geographically related peridotites despite both limited melt depletion and susceptibility to recent Re mobility, is to use linear trends defined by variable $^{187}Os/^{188}Os$ and immobile indicators of melt depletion (e.g., $Al_2O_3$, CaO or Lu) as isochron analogues. The immobile element concentrations serve as proxies for Re/Os (Reisberg and Lorand, 1995) given that in most instances, these elements are much less susceptible to recent alteration and contamination than Re. This method assumes a single-stage of melt depletion and requires an assumption to be made with regard to the $Al_2O_3$, CaO or Lu concentration of the residue at the point of complete Re removal. Handler and Bennett (1999) argued that extrapolation to $Al_2O_3$ of 0.7 wt% is warranted because in most peridotite suites worldwide Re/Os approaches zero at that approximate level of depletion.

An additional question related to the melt depletion age is its extent affected by mixing/metasomatic processes. It is generally thought that it is impossible to mix lithospheric mantles which show different melt depletion ages since they are rigid in rheology. Theoretically, the metasomatism by aqueous agent or melt could elevate the $^{187}Os/^{188}Os$ ratio, hence decrease the melt depletion age, due to its high $^{187}Re/^{188}Os$ ratio. However, it is usually thought that the metasomatic fluids or melts are mostly silicate and contain too low Os content to result in significant elevation of $^{187}Os/^{188}Os$ ratio of metasomatized mantle (Shirey and Walker, 1998; Walker et al., 2002; Chesley et al., 2004). However, in order to avoid possible effect, harzburgite is usually used to get more reliable melt depletion age due to its low Re concentration and fact that the harzburgite would transformed into lherzolite if it was intensively metasomatized by fluid and melt.

## Appendix B. Supplementary data

Supplementary data associated with this article can be found, in the online version, at doi:10.1016/j.gca.2006.07.014.

## References


Alard, O., Griffin, W.L., Pearson, N.J., Lorand, J.P., O'Reilly, S.Y., 2002. New insights into the Re–Os systematics of sub-continental lithospheric mantle from in situ analysis of sulphides. *Earth Planet. Sci. Lett.* **203**, 651–663.

Alard, O., Luguet, A., Pearson, N.J., Griffin, W.L., Lorand, J.P., Gannoun, A., Burton, K.W., O'Reilly, S.Y., 2005. In situ Os isotopes in abyssal peridotites bridge the isotopic gap between MORBs and their source mantle. *Nature* **436**, 1005–1008.

Aulbach, S., Griffin, W.L., Pearson, N.J., O'Reilly, S.Y., Kivi, K., Doyle, B.J., 2004. Mantle formation and evolution, Slave Craton: constraints from HSE abundances and Re-Os isotope systematics of sulfide inclusions in mantle xenocrysts. *Chem. Geol.* **208**, 61–88.

Bao, X.Z., Guan, Y.X., Wang, G.Q., Huang, S.F., 1995. Two kinds of chemical composition zoning trends and their genesis in Cr-spinel from kimberlites, Wafangdian area (in Chinese with English abstract). *J. Changchun Uni. Earth Sci.* **25**, 381–386.

Beck, S.L., Zandt, G., 2002. The nature of orogenic crust in central Andes. *J. Geophys. Res.* **107**. doi:10.1029/2000JB00012.

Bertrand, P., Mercier, J.C., 1985. The mutual solubility of coexisting ortho- and clinopyroxene: toward an absolute geothermometer for the natural system? *Earth Planet. Sci. Lett.* **76**, 109–122.

Bird, P., 1979. Continental delamination and the Colorado Plateau. *J. Geophys. Res.* **84**, 7561–7571.

Bodinier, J.-L., Vasseur, G., Vernieres, J., Dupuy, C., Fabries, J., 1990. Mechanisms of mantle metasomatism: geochemical evidence from the Lherz orogenic peridotite. *J. Petrol.* **31**, 597–628.

Boyd, F.R., 1989. Compositional distinction between oceanic and cratonic lithosphere. *Earth Planet. Sci. Lett.* **96**, 15–26.

Boyd, F.R., Pokhilenko, N.P., Pearson, D.G., Mertzman, S.A., Sobolev, N.V., Finger, L.W., 1997. Composition of the Siberian cratonic mantle: evidence from Udachnaya peridotite xenoliths. *Contrib. Mineral. Petrol.* **128**, 228–246.

Brandon, A.D., Creaser, R.A., Shirey, S.B., Carlson, R.W., 1996. Osmium recycling in subduction zones. *Science* **272**, 861–864.

Brandon, A.D., Becker, H., Carlson, R.W., Shirey, S.B., 1999. Isotopic constraints on time scales and mechanisms of slab material transport in the mantle wedge: evidence from the Simcoe mantle xenoliths, Washington, USA. *Chem. Geol.* **160**, 387–408.

Brandon, A.D., Snow, J.E., Walker, R.J., Morgan, J.W., Mock, T.D., 2000. $^{190}Pt$–$^{186}Os$ and $^{187}Re$–$^{187}Os$ systematics of abyssal peridotites. *Earth Planet. Sci. Lett.* **177**, 319–335.

Brey, G.P., Kohler, T., 1990. Geothermobarometry in four-phase lherzolites II: new thermobarometers, and practical assessment of existing thermobarometers. *J. Petrol.* **31**, 1353–1378.

Carlson, R.W., Irving, A.J., 1994. Depletion and enrichment history of subcontinental lithospheric mantle: an Os, Sr, Nd and Pb isotopic study of ultramafic xenoliths from the northwestern Wyoming Craton. *Earth Planet. Sci. Lett.* **126**, 457–472.

Carlson, R.W., Irving, A.J., Hearn, Jr. B.C., 1999. Chemical and isotopic systematics of peridotite xenoliths from the Williams kimberlite, Montana: clues to processes of lithosphere formation, modification and destruction. In: Gurney, J.J. Gurney, J.L., Pascoe, M.D., Richardson, S,H. (eds.), *Proceedings of the Seventh International Kimberlite Conference*. Cape Town, South Africa, pp. 90–98.

Carlson, R.W., Boyd, F.R., Shirey, S.B., thirteen others, 2000. Continental growth, preservation, and modification in Southern Africa. GSA Today 10 (2), 1–7.

Carlson, R.W., Pearson, D.G., James, D.E., 2005. Physical, chemical, and chronological characteristics of continental mantle. *Rev. Geophys.* **43**, 2004RG000156.

Chen, B., Zhai, M.G., 2003. Geochemistry of late Mesozoic lamprophyre dykes from the Taihang Mountains, north China, and implications for the sub-continental lithospheric mantle. *Geol. Mag.* **140**, 87–93.

Chen, B., Jahn, B.M., Arakawa, Y., Zhai, M.G., 2004. Petrogenesis of the Mesozoic intrusive complexes from the southern Taihang orogen, north China Craton: elemental and Sr–Nd–Pb isotopic constraints. *Contrib. Mineral. Petrol.* **148**, 489–501.

Chesley, J.T., Rudnick, R.L., Lee, C.T., 1999. Re-Os systematics of mantle xenoliths from the east African rift: Age, structure, and history of the Tanzanian craton. *Geochim. Cosmochim. Acta* **63**, 1203–1217.

Chesley, J., Righter, K., Ruiz, J., 2004. Large-scale mantle metasomatism: a Re–Os perspective. *Earth Planet. Sci. Lett.* **219**, 49–60.

Chi, J.S., 1988. *The study of Cenozoic basalts and upper mantle beneath eastern China*. China University of Geosciences Publishing House, Wuhan, p. 277.

Chi, J.S., Lu, F.X., 1996. *Kimberlites and the features of Paleozoic lithospheric mantle in North China craton*. Science Press, Beijing, p. 292.

Cohen, A.S., Waters, F.G., 1996. Separation of osmium from geological materials by solvent extraction for analysis by TIMS. *Anal. Chim. Acta* **332**, 269–275.

Davies, G., 1994. Thermomechanical erosion of the lithosphere by mantle plume. *J. Geophys. Res.* **99**, 15709–15722.

Deng, J.F., Mo, X.X., Zhao, H.L., Luo, Z.H., Du, Y.S., 1994. Lithosphere root/de-rooting and activation of the east China continent (in Chinese with English abstract). *Geoscience* **8**, 349–356.

Dobbs, P.N., Duncan, D.J., Hu, S., Shee, S.R., Colgan, E.A., Brown, M.A., Smith, C.B., Allsopp, H.P., 1994. The geology of Mengyin kimberlites, Shandong, China. In: Meyer, O.A., Leonardos, O.H. (eds.), *Kimberlites, Related Rocks and Mantle Xenoliths*. CPRM Spec. Publ., 1A/93, pp. 40–61.

Doin, M.P., Fleitout, L., Christensen, U., 1997. Mantle convection and the stability of depleted and undepleted continental lithosphere. *J. Geophys. Res.* **102**, 2771–2787.

Downes, H., 2001. Formation and modification of the shallow subcontinental lithospheric mantle: a review of geochemical evidence from ultramafic xenolith suites and tectonically emplaced ultramafic massifs of Western and Central Europe. *J. Petrol.* **42**, 233–250.

E, M.L., Zhao, D.S., 1987. *Cenozoic Basalts and Deep-seated Rock Xenoliths in Eastern China*. Science Press, Beijing, p. 490.

Fan, Q.C., Hooper, P.R., 1989. The mineral chemistry of ultramafic xenoliths of eastern China: implications for upper mantle composition and the paleogeotherms. *J. Petrol.* **30**, 1117–1158.

Fan, W.M., Menzies, M.A., 1992. Destruction of aged lower lithosphere and accretion of asthenosphere mantle beneath eastern China. *Geotectonica Metallogenia* **16**, 171–180.

Fan, W.M., Zhang, H.F., Baker, J., Jarvis, K.E., Mason, P.R.D., Menzies, M.A., 2000. On and off the North China Craton: where is the Archean keel? *J. Petrol.* **41**, 933–950.

Fang, T.H., Ma, H.W., 1999. Composition and thermal structure of the upper mantle lithosphere beneath Kuandian area, Liaoning Province (in Chinese with English abstract). *Geol. Rev.* **45** (Supp.), 450–457.

Faure, M., Lin, W., Monie, P., Bruguier, O., 2004. Palaeoproterozoic arc magmatism and collision in Liaodong Peninsula (north-east China). *Terra Nova* **16**, 75–80.

Flesch, L.M., Holt, W.E., Silver, P.G., Stevenson, M., Wang, C.Y., Chan, W.W., 2005. Constraining the extent of crust-mantle coupling in central Asia using GPS, geologic, and shear wave splitting data. *Earth Planet. Sci. Lett.* **238**, 248–268.

Fouch, M.J., 2000. Shear wave splitting, continental keels, and patterns of mantle flow. *J. Geophys. Res.* **105**, 6255–6276.

Gao, S., Zhang, B.R., Luo, T.C., Li, Z.J., Xie, Q.L., Gu, X.M., Zhang, H.F., Ouyang, J.P., Wang, D.P., Gao, C.L., 1992. Chemical composition of the continental crust in the Qinling Orogenic Belt and its adjacent North China and Yangtze Cratons. *Geochim. Cosmochim. Acta* **56**, 3933–3950.

Gao, S., Zhang, B.R., Jin, Z.M., Kern, H., Luo, T.C., Zhao, Z.D., 1998. How mafic is the lower continental crust? *Earth Planet. Sci. Lett.* **161**, 101–117.

Gao, S., Rudnick, R.L., Carlson, R.W., McDonough, W.F., Liu, Y.S., 2002a. Re–Os evidence for replacement of ancient mantle lithosphere beneath the North China Craton. *Earth Planet. Sci. Lett.* **198**, 307–322.

Gao, S., Liu, X.M., Yuan, H.L., Hattendorf, B., Gunther, D., Chen, L., Hu, S.H., 2002b. Determination of forty two major and trace elements in USGS and NIST SRM glasses by laser-inductively coupled plasma-mass spectrometry. *Geostand. Newsl.* **26**, 181–196.

Gao, S., Rudnick, R.L., Yuan, H.L., Liu, X.M., Liu, Y.S., Xu, W.L., Ling, W.L., Ayers, J., Wang, X.C., Wang, Q.H., 2004. Recycling lower continental crust in the North China craton. *Nature* **432**, 892–897.

Griffin, W.L., Zhang, A.-D., O'Reilly, S.Y., Ryan, C.G., 1998. Phanerozoic evolution of the lithosphere beneath the Sino-Korean craton. In: Flower, M.F.J., Chung, S.-L., Lo, C.-H., Lee, T.-Y. (eds.), *Mantle Dynamics and Plate Interactions in East Asia*. Am. Geophy. Union, Washington, D.C., Geodyn. Ser. 27, pp. 107–126.

Griffin, W.L., O'Reilly, S.Y., Ryan, C.G., 1999a. The composition and origin of subcontinental lithospheric mantle. In: Fei, Y., Bertka, C.M., Mysen, B.O. (Eds.), *Mantle Petrology: Field Observations and High-pressure Experimentation: A Tribute to Francis R. (Joe) Boyd*. The Geochemical Society, Special Publication 6, pp. 13–43.

Griffin, W.L., Doyle, B.J., Ryan, C.G., Pearson, N.J., O'Reilly, S.Y., Davies, R., Kikv, K., Van Achterbergh, E., Natapov, L.M., 1999b. Layered mantle lithosphere in the Lac de Gras Area, Slave Craton: composition, structure and origin. *J. Petrol.* **40**, 705–727.

Guo, F., Fan, W.M., Wang, Y.J., Lin, G., 2001. Late Mesozoic intrusive complexes in the North China Block: constraints on the nature of subcontinental lithospheric mantle. *Phy. Chem. Earth (A)* **26**, 759–771.

Guo, F., Fan, W.M., Wang, Y.J., Lin, G., 2003. Geochemistry of late Mesozoic mafic magmatism in west Shandong Province, eastern China: characterizing the losing lithospheric mantle beneath the North China Block. *Geochem. J.* **37**, 63–77.

Hacker, B.R., Ratschbacher, L., Webb, L., Ireland, T., Walker, D., Dong, S.W., 1998. U/Pb zircon ages constrain the architecture of the

ultrahigh-pressure Qinling-Dabie Orogen, China. *Earth Planet. Sci. Lett.* **161**, 215–230.

Handler, M.R., Bennett, V.C., 1999. Behaviour of platinum-group elements in the subcontinental mantle of eastern Australia during variable metasomatism and melt depletion. *Geochim. Cosmochim. Acta* **63**, 3597–3618.

Handler, M.R., Bennett, V.C., Carlson, R.W., 2005. Nd, Sr and Os isotope systematics in young, fertile spinel peridotite xenoliths from northern Queensland, Australia: a unique view of depleted MORB mantle? Geochim. *Cosmochim. Acta* **69**, 5747–5763.

Harvey, J., Gannoun, A., Burton, K.W., Rogers, N.W., Alard, O., Parkinson, I.J., 2006. Ancient melt extraction from the oceanic upper mantle revealed by Re–Os isotopes in abyssal peridotites from the Mid-Atlantic ridge. *Earth Planet. Sci. Lett.* **244**, 606–621.

Ionov, D.A., O'Reilly, S.Y., Griffin, W.L., 1997. Volatile-bearing minerals and lithophile trace elements in the upper mantle. *Chem. Geol.* **141**, 153–184.

Irvine, G.J., Pearson, D.G., Kjarsgaard, B.A., Carlson, R.W., Kopylova, M.G., Dreibus, G., 2003. A Re–Os isotope and PGE study of kimberlite-derived peridotite xenoliths from Somerset Island and a comparison to the Slave and Kaapvaal cratons. *Lithos* **71**, 461–488.

Jordan, T.H., 1988. Structure and formation of the continental tectosphere. *J. Petrol. (Special Lithosphere Issue)*, 11–37.

Kay, R.W., Kay, S.M., 1993. Delamination and delamination magmatism. *Tectonophysics* **219**, 177–189.

Klemme, S., O'Neill, H.S.C., 2000. The near-solidus transition from garnet lherzolite to spinel lherzolite. *Contrib. Mineral. Petrol.* **138**, 237–248.

Kopylova, M.G., Russell, J.K., 2000. Chemical stratification of cratonic lithosphere: constraints from the northern Slave craton, Canada. *Earth Planet. Sci. Lett.* **181**, 71–87.

LBGMR (Liaoning Bureau of Geology and Mineral Resources), 1989. *Regional Geology of Liaoning Province* (in Chinese with English summary). Geological Publishing House, Beijing, pp. 317–520.

Lee, C.T., Yin, Q.Z., Rudnick, R.L., Chesley, J.T., Jacobsen, S.B., 2000. Osmium isotopic evidence for Mesozoic removal of lithospheric mantle beneath the Sierra Nevada, California. *Science* **289**, 1912–1916.

Lee, C.T., Yin, Q.Z., Rudnick, R.L., Jacobsen, S.B., 2001. Preservation of ancient and fertile lithospheric mantle beneath the southwestern United States. *Nature* **411**, 69–73.

Lee, S.R., Walker, R.J., 2006. Re–Os isotope systematics of mantle xenoliths from South Korea: evidence for complex growth and loss of lithospheric mantle beneath East Asia. *Chem. Geol.* **231**, 90–101.

Lenardic, A., Moresi, L.N., Muhlhaus, H., 2003. Longevity and stability of cratonic lithosphere: insights from numerical simulations of coupled mantle convection and continental tectonics. *J. Geophys. Res.* **108**. doi:10.1029/2002JB00185.

Lindsley, D.H., Dixon, S.A., 1975. Diopside-enstatite equilibria at 850 °C to 1400 °C, 5 to 35 kbar. *Am. J. Sci.* **276**, 1282–1301.

Liu, C.Q., Masuda, A., Xie, G.H., 1992. Isotope and trace-element geochemistry of alkali basalts and associated megacrysts from the Huangyishan volcano, Kuandian, Liaoning, NE China. *Chem. Geol.* **97**, 219–231.

Liu, D.Y., Nutman, A.P., Compston, W., Wu, J.S., Shen, Q.H., 1992. Remmants of $\geqslant$3800 Ma crust in the Chinese part of the Sino-Korean Craton. *Geology* **20**, 339–342.

Lu, F.X., E, M.L., Deng, J.F., 1983. Ultramafic xenoliths and megacrysts in alkaline basalts from Huangyishan, Kuandian, Liaoning Province, China (in Chinese with English abstract). *Petrol. Res.* **3**, 77–88.

Lu, F.X., Zhao, L., Deng, J.F., Zheng, J.P., 1995. Disssion on the ages of kimberlitic magma activity in the North China Platform (In Chinese with English abstract). *Acta Petrol. Sinica* **11**, 355–374.

Lu, X.P., Wu, F.Y., Guo, J.H., Wilde, S.A., Yang, J.H., Liu, X.M., Zhang, X.O., 2006. Zircon U-Pb geochronological constraints on the Paleoproterozoic crustal evolution of the Eastern Block in the North China Craton. *Precambrian Res.* **146**, 138–164.

Luo, Y., Sun, M., Zhao, G.C., Li, S.Z., Xu, P., Ye, K., Xia, X.P., 2004. LA-ICP-MS U–Pb zircon ages of the Liaohe Group in the Eastern Block of the North China Craton: constraints on the evolution of the Jiao-Liao-Ji Belt. *Precambrian Res.* **134**, 349–371.

Lustrino, M., 2005. How the delamination and detachment of lower crust can influence basaltic magmatism. *Earth Sci. Rev.* **72**, 21–38.

McDonough, W.F., Stosch, H.G., Ware, N., 1992. Distribution of titanium and the rare earth elements between peridotitic minerals. *Contrib. Mineral. Petrol.* **110**, 321–328.

Meen, J.K., Eggler, D.H., Ayers, J.C., 1989. Experimental evidence for very solubility of REE in CO2-fluids under mantle conditions. *Nature* **340**, 301–303.

Meibom, A., Sleep, N.H., Chamberlain, C.P., Coleman, R.G., Frei, R., Hren, M.T., Wooden, J.L., 2002. Re-Os isotopic evidence for long-lived heterogeneity and equilibration processes in Earth's upper mantle. *Nature* **419**, 705–708.

Meisel, T., Walker, R.J., Irving, A.J., Lorand, J.-P., 2001. Osmium isotopic compositions of mantle xenoliths: a global perspective. *Geochim. Cosmochim. Acta* **65**, 1311–1323.

Menzies, M.A., Xu, Y.G., 1998. Geodynamics of the North China Craton. In: Flower, M.F.J., Chung, S.-L., Lo, C.-H., Lee, T.-Y. (eds.), *Mantle Dynamics and Plate Interactions in East Asia.* Am. Geophy. Union, Washington, DC, Geodyn. Ser. 27, pp. 155–165.

Menzies, M.A., Fan, W.M., Zhang, M., 1993. Palaeozoic and Cenozoic lithoprobe and the loss of >120 km of Archean lithosphere, Sino-Korean craton, China. In: Prichard, H.M., Alabaster, T., Harris, N.B.W., Neary, C.R. (eds.), *Magmatic Processes and Plate Tectonic.* Geol. Soc. Special Publ. 76, pp. 71–81.

Nehru, C.E., Wyllie, P.J., 1974. Eletron-microprobe measurement of pyroxene coexisting with $H_2O$-undersaturated liquid in the join $CaMgSi_2O_6$–$Mg_2Si_2O$–$H_2O$ at 30 kbar with application to geothermometry. *Contrib. Mineral. Petrol.* **48**, 221–228.

O'Reilly, S.Y., Griffin, W.L., Poudjom Djomani, Y.H., Morgan, P., 2001. Are lithospheres forever? *GSA Today* **11** (4), 4–10.

Palme, H., O'Neill, H.S.C., 2003. Cosmochemical estimates of mantle composition. In: Carlson, R.W. (Ed.), *Treatise on Geochemistry. The Mantle and Core*, vol. 2. Elsevier, pp. 1–38.

Pearson, D.G., Canil, D., Shirey, S.B., 2003. Mantle samples included in volcanic rocks: xenoliths and diamonds. In: Carlson, R.W. (ed.), *Treatise on Geochemistry: The Mantle and Core* 2, pp. 171–276.

Peslier, A.H., Reisberg, L., Ludden, J., Francis, D., 2000a. Os isotopic systematics in mantle xenoliths; age constraints on the Canadian Cordillera lithosphere. *Chem. Geol.* **166**, 85–101.

Peslier, A.H., Reisberg, L., Ludden, J., Francis, D., 2000b. Re-Os constraints on harzburgite and lherzolite formation in the lithospheric mantle: a study of northern Canadian Cordillera xenoliths. *Geochim. Cosmochim. Acta* **64**, 3061–3071.

Poudjom Djomani, Y.H., O'Reilly, S.Y., Griffin, W.L., Morgan, P., 2001. The density structure of subcontinental lithosphere through time. *Earth Planet. Sci. Lett.* **184**, 605–621.

Pysklywec, R.N., Beaumont, C., Fullsack, P., 2000. Modeling the behaviour of the continental mantle lithosphere during plate convergence. *Geology* **28**, 655–659.

Rampone, E., Botazzi, P., Ottolini, L., 1991. Complementary Ti and Zr anomalies in orthopyroxene and clinopyroxene from mantle peridotites. *Nature* **354**, 518–520.

Reisberg, L.C., Lorand, J.-P., 1995. Longevity of sub-continental mantle lithosphere from osmium isotope systematics in orogenic peridotite massifs. *Nature* **376**, 159–162.

Reisberg, L., Lorand, J.-P., Bedini, R.M., 2004. Reliability of Os model ages in pervasively metasomatized continental mantle lithosphere: a case study of Sidamo spinel peridotite xenoliths (East African Rift, Ethiopia). *Chem. Geol.* **208**, 119–140.

Reisberg, L., Zhi, X.C., Lorand, J.-P., Wagner, C., Peng, Z.C., Zimmermann, C., 2005. Re–Os and S systematics of spinel peridotite xenoliths from east central China: Evidence for contrasting effects of melt percolation. *Earth Planet. Sci. Lett.* **239**, 286–308.

Sachtleben, Th., Seck, H.A., 1981. Chemical control of Al-solubility in orthopyroxene and its implications on pyroxene geothermometry. *Contrib. Mineral. Petrol.* **78**, 157–165.

Shirey, S.B., Walker, R.J., 1995. Carius tube digestions for low-blank rhenium–osmium analysis. *Anal. Chem.* **67**, 2136–2141.

Shirey, S.B., Walker, R.J., 1998. The Re–Os isotope system in cosmochemistry and high temperature geochemistry. *Ann. Rev. Earth Planet. Sci.* **26**, 423–500.

Sleep, N.H., 2005. Evolution of the continental lithosphere. *Annu. Rev. Earth Planet. Sci.* **33**, 369–393.

Snow, J.E., Reisberg, L., 1995. Os isotopic systematics of the MORB mantle: results from altered abyssal peridotites. *Earth Planet. Sci. Lett.* **136**, 723–733.

Sun, S.S., McDonough, W.F., 1989. Chemical and isotopic systematics of oceanic basalts: Implications for mantle composition and processes. In: Saunders, A.D., Norry, M.J. (ed.), *Magmatism in the Ocean Basins.* Geol. Soc. Special Pub. 42, pp. 313–345.

Tapponnier, P., Peltzer, G., Ledain, A.Y., Armigo, R., Cobbold, P., 1982. Propagating extrusion tectonics in Asia—new insights from simple experiments with plasticine. *Geology* **10**, 611–616.

Tatsumoto, M., Basu, A.R., Huang, W.K., Wang, J.W., Xie, G.H., 1992. Sr, Nd, and Pb isotopes of ultramafic xenoliths in volcanic rocks of Eastern China: enriched components EMI and EMII in subcontinental lithosphere. *Earth Planet. Sci. Lett.* **113**, 107–128.

Walker, R.J., Carlson, R.W., Shirey, S.B., Boyd, F.R., 1989. Os, Sr, Nd, and Pb isotope systematics of southern African peridotite xenoliths: Implications for the chemical evolution of subcontinental mantle. *Geochim. Cosmochim. Acta* **53**, 1583–1595.

Walker, R.J., Morgan, J.W., Horan, M.F., Czamanske, G.K., Krogstad, E.J., Fedorenko, V.A., Kunilov, V.E., 1994. Re-Os isotopic evidence for an enriched-mantle source for the Noril'sk-type, ore-bearing intrusions, Siberia. *Geochim. Cosmochim. Acta* **58**, 4179–4197.

Walker, R.J., Stone, W.R., 2001. Os isotope constraints on the origin of the 2.7 Ga Boston Creek flow, Ontario, Canada. *Chem. Geol.* **175**, 567–579.

Walker, R.J., Prichard, H.M., Ishiwatari, A., Pimentel, M., 2002. The osmium isotopic composition of convecting upper mantle deduced from ophiolite chromites. *Geochim. Cosmochim. Acta* **66**, 329–345.

Walter, M.J., 2003. Melt extraction and compositional variability in mantle lithosphere. In: Carlson, R.W. (Ed.), *Treatise on Geochemistry: The Mantle and Core*, vol. 2. Elsevier, pp. 363–394.

Wang, W.Y., Takahashi, E., Sueno, S., 1998. Geochemical properties of lithospheric mantle beneath the Sino-Korea craton; evidence from garnet xenocrysts and diamond inclusions. *Phys. Earth Planet. Interiors* **107**, 249–260.

Wells, P.R.A., 1977. Pyroxene thermometry in simple and complex systems. *Contrib. Mineral. Petrol.* **62**, 129–139.

Wood, B.J., Banno, S., 1973. Garnet-orthopyroxene and orthopyroxene–clinopyroxene relationships in simple and complex systems. *Contrib. Mineral. Petrol.* **42**, 109–124.

Wu, F.Y., Sun, D.Y., 1999. The Mesozoic magmatism and lithospheric thinning in Eastern China (in Chinese with English abstract). *J. Changchun Uni. Sci. Tech.* **29**, 313–318.

Wu, F.Y., Sun, D.Y., Zhang, G.L., Ren, X.W., 2000. Deep geodynamics of Yanshain Movement (in Chinese with English abstract). *Geol. J. China Uni.* **6**, 379–388.

Wu, F.Y., Walker, R.J., Ren, X.W., Sun, D.Y., Zhou, X.H., 2003. Osmium isotopic constraints on the age of lithospheric mantle beneath northeastern China. *Chem. Geol.* **197**, 107–129.

Wu, F.Y., Zhao, G.C., Wilde, S.A., Sun, D.Y., 2005a. Nd Isotopic constraints on the crustal formation of the North China Craton. *J. Asian Earth Sci.* **24**, 523–545.

Wu, F.Y., Lin, J.Q., Wilde, S.A., Zhang, X.O., Yang, J.H., 2005b. Nature and significance of the Early Cretaceous giant igneous event in Eastern China. *Earth Planet. Sci. Lett.* **233**, 103–119.

Wu, F.Y., Yang, J.H., Wilde, S.A., Zhang, X.O., 2005c. Geochronology, petrogenesis and tectonic implications of Jurassic granites in the Liaodong Peninsula, NE China. *Chem. Geol.* **221**, 127–156.

Xie, G.H., Wang, J.W., Wei, K.J., Liu, C.Q., 1992. The study on geochemistry of Cenozoic volcanic rock in Huangyishan, Kuandian, Liaoning Province (in Chinese). In: Liu, R.X. (Ed.), *The age and geochemistry of Cenozoic volcanic rocks in China*. Seismic Press, Beijing, pp. 101–113.

Xu, S., Nagao, K., Uto, K., Waki ta, H., Nakai, S., Liu, C.Q., 1998. He, Sr and Nd isotopes of mantle-derived xenoliths in volcanic rocks of NE China. *J. Asian Earth Sci.* **16**, 547–556.

Xu, Y.G., 2001. Thermo-tectonic destruction of the Archean lithospheric keel beneath eastern China: evidence, timing and mechanism. *Phy. Chem. Earth (A)* **26**, 747–757.

Xu, Y.G., Menzies, M.A., Thirlwall, M.F., Xie, G.H., 2001. Exotic lithosphere beneath the Western Yangtze Craton: Petrogenetic links to Tibet using highly magnesian ultrapotassic rocks. *Geology* **29**, 863–866.

Xu, Y.G., Huang, X.L., Ma, J.L., Wang, Y.B., Iizuka, Y., Xu, J.F., Wang, Q., Wu, X.Y., 2004. Crust-mantle interaction during the tectono-thermal reactivation of the North China Craton: constraints from SHRIMP zircon U–Pb chronology and geochemistry of Mesozoic plutons from western Shandong. *Contrib. Mineral. Petrol.* **147**, 750–767.

Yaxley, G.M., Green, D.H., Kamenetsky, V., 1998. Carbonatite metasomatism in the southeastern Australian lithosphere. *J. Petrol.* **39**, 1917–1930.

Ye, K., Cong, B.L., Ye, D.N., 2000. The possible subduction of continental material to depths greater than 200 km. *Nature* **407**, 734–736.

Yu, C.X., 1987. Geological characters of kimberlite in northern Liaoning (in Chinese with English abstract). *Liaoning Geol.* **No. 3**, 228–237.

Yuen, D.A., Fleitout, L., 1985. Thinning of the lithosphere by small-scale convective destabilization. *Nature* **313**, 125–128.

Zhang, H.F., Sun, M., Zhou, X.H., Zhou, M.F., Fan, W.M., Zheng, J.P., 2003. Secular evolution of the lithosphere beneath the eastern North China Craton: evidence from Mesozoic basalts and high-Mg andesites. *Geochim. Cosmochim. Acta* **67**, 4373–4387.

Zhang, H.F., Sun, M., Zhou, M.F., Fan, W.M., Zhou, X.H., Zhai, M.G., 2004. Highly heterogeneous late Mesozoic lithospheric mantle beneath the North China Craton: evidence from Sr–Nd–Pb isotopic systematics of mafic igneous rocks. *Geol. Mag.* **141**, 55–62.

Zhang, H.F., 2005. Transformation of lithospheric mantle through peridotite-melt reaction: A case of Sino-Korean craton. *Earth Planet. Sci. Lett.* **237**, 768–780.

Zhao, D.G., 1998. *Kimberlites, diamonds and mantle xenoliths from the north China craton and the Canadian northwest territories*. Ph D. dissertation, University of Michigan, 220pp.

Zhao, G.C., Sun, M., Wilde, S.A., Li, S.Z., 2005. Late Archean to Paleoproterozoic evolution of the North China Craton: key issues revisited. *Precambrian Res.* **136**, 177–202.

Zheng, J.P., 1999. *Mesozoic–Cenozoic mantle replacement and lithospheric thinning beneath the eastern China* (in Chinese with English abstract). China Uni. Geosci. Press, Wuhan, p. 126.

Zheng, J.P., O'Reilly, S.Y., Griffin, W.L., Lu, F.X., Zhang, M., Pearson, N.J., 2001. Relict refractory mantle beneath the eastern North China block: significance for lithosphere evolution. *Lithos* **57**, 43–66.

Zheng, J.P., Griffin, W.L., O'Reilly, S.Y., Lu, F.X., Yu, C.M., Zhang, M., Li, H.M., 2004. U–Pb and Hf-isotope analysis of zircons in mafic xenoliths from Fuxian kimberlites: evolution of the lower crust beneath the North China craton. *Contrib. Mineral. Petrol.* **148**, 79–103.

Zhi, X.C., Peng, Z.C., Chen, D.G., Yu, C.J., Sun, W.D., Reisberg, L., 2001. The longevity of subcontinental lithospheric mantle beneath Jiangsu-Anhui region. *Sci. China (Ser. D)* **44**, 1110–1118.

Zhi, X.C., Qin, X., 2004. Re-Os isotope geochemistry of the mantle-derived peridotite xenoliths from eastern China: constrains on the age and thinning of lithospheric mantle. *Acta Petrol. Sinica* **20**, 989–998.

Zhou, X.H., Zhu, B.Q., Liu, R.X., Chen, W.J., 1988. Cenozoic basaltic rocks in eastern China. In: MacDougall, J.D. (Ed.), *Continental Flood Basalt*. Kluwer, Dordrecht, pp. 311–330.